Atmospheric
Chemistry
and Physics
Discussions

Open Access

Aura OMI observations of regional SO$_2$ and NO$_2$ pollution changes from 2005 to 2014

N. A. Krotkov[1], C. A. McLinden[2], C. Li[3,1], L. N. Lamsal[4,1], E. A. Celarier[4,1], S. V. Marchenko[5,1], W. H. Swartz[6,1], E. J. Bucsela[7], J. Joiner[1], B. N. Duncan[1], K. F. Boersma[8,9,10], J. P. Veefkind[9,11], P. F. Levelt[9,11], V. E. Fioletov[2], R. R. Dickerson[12], H. He[12], Z. Lu[13], and D. G. Streets[13]

[1]Atmospheric Chemistry and Dynamics Laboratory, NASA Goddard Space Flight Center, Greenbelt, Maryland, USA
[2]Air Quality Research Division, Environment Canada, Toronto, Canada
[3]Earth System Science Interdisciplinary Center, University of Maryland, College Park, USA
[4]GESTAR, Universities Space Research Association, Columbia, Maryland, USA
[5]Science Systems and Applications, Inc., Lanham, Maryland, USA
[6]Applied Physics Laboratory, Johns Hopkins University, Laurel, Maryland, USA
[7]SRI International, Menlo Park, California, USA
[8]Meteorology and Air Quality Group, Wageningen University, Wageningen, the Netherlands
[9]Royal Netherlands Meteorological Institute, De Bilt, the Netherlands

ACPD

15, 26555–26607, 2015

Aura OMI observations of regional SO$_2$ and NO$_2$ pollution changes

N. A. Krotkov et al.

Title Page

Abstract	Introduction
Conclusions	References
Tables	Figures

|◄ | ►|
◄ | ►
Back | Close

Full Screen / Esc

Printer-friendly Version

Interactive Discussion

[10]Department of Applied Physics, Eindhoven University of Technology, Eindhoven, the Netherlands
[11]University of Technology Delft, Delft, the Netherlands
[12]Department of Atmospheric and Oceanic Science, University of Maryland, College Park, Maryland, USA
[13]Energy Systems Division, Argonne National Laboratory, Argonne, IL, USA

Correspondence to: N. A. Krotkov (nickolay.a.krotkov@nasa.gov)

Title Page

Abstract | Introduction

Conclusions | References

Tables | Figures

|◄ | ►|

◄ | ►

Back | Close

Full Screen / Esc

Printer-friendly Version

Interactive Discussion

Abstract

The Ozone Monitoring Instrument (OMI) onboard NASA's Aura satellite has been providing global observations of the ozone layer and key atmospheric pollutant gases, such as nitrogen dioxide (NO$_2$) and sulfur dioxide (SO$_2$), since October 2004. The data

5 products from the same instrument provide consistent spatial and temporal coverage and permit the study of anthropogenic and natural emissions on local-to-global scales. In this paper we examine changes in SO$_2$ and NO$_2$ over some of the world's most polluted industrialized regions during the first decade of OMI observations. In terms of regional pollution changes, we see both upward and downward trends, sometimes in

10 opposite directions for NO$_2$ and SO$_2$, for the different study areas. The trends are, for the most part, associated with economic and/or technological changes in energy use, as well as regional regulatory policies. Over the eastern US, both NO$_2$ and SO$_2$ levels decreased dramatically from 2005 to 2014, by more than 40 and 80 %, respectively, as a result of both technological improvements and stricter regulations of emissions. OMI

15 confirmed large reductions in SO$_2$ over eastern Europe's largest coal power plants after installation of flue gas desulfurization devices. The North China Plain has the world's most severe SO$_2$ pollution, but a decreasing trend has been observed since 2011, with about a 50 % reduction in 2012–2014, due to an economic slowdown and government efforts to restrain emissions from the power and industrial sectors. In contrast, India's

20 SO$_2$ and NO$_2$ levels from coal power plants and smelters are growing at a fast pace, increasing by more than 100 and 50 %, respectively, from 2005 to 2014. Several SO$_2$ hot spots observed over the Persian Gulf are probably related to oil and gas operations and indicate a possible underestimation of emissions from these sources in bottom-up emission inventories. Overall, OMI observations have proved to be very valuable in

25 documenting rapid changes in air quality over different parts of the world during the last decade. The baseline established during the first 10 years of OMI is indispensable for the interpretation of air quality measurements from current and future satellite atmospheric composition missions.

1 Introduction

Sulfur dioxide (SO_2) and nitrogen dioxide (NO_2) are reactive, short-lived atmospheric trace gases with both anthropogenic and natural sources. Major sources of NO_x ($NO_x = NO + NO_2$) include fossil fuel combustion, biomass burning, soil emissions (Vinken et al., 2014b) and lightning (Schumann and Huntrieser, 2007). NO_2 partici-
pates in the nitrogen cascade of air–water–soil (EPA, 2011; Galloway et al., 2013), affects atmospheric oxidation rates (Valin et al., 2013), and contributes to surface ozone production (Duncan et al., 2010; Seinfeld and Pandis, 2006). The principal sources of SO_2 are natural volcanic and anthropogenic emissions from burning sulfur-contaminated fossil fuels and the refinement of sulfide ores. Volcanic SO_2 is often in-
jected into the atmosphere at high altitudes above the planetary boundary layer (PBL), while anthropogenic SO_2 emissions are predominantly in or slightly above the PBL. Chemical reactions in the PBL involving SO_2 and NO_2 lead to the production of aerosol oxidation products (sulfate and nitrate aerosols), and tropospheric ozone (Seinfeld and Pandis, 2006). Volatile Organic Compounds (VOCs) oxidize in the presence of NO_x
and sunlight to form ozone (O_3), a major tropospheric pollutant and greenhouse gas (EPA, 2013), and the oxidation product of NO_2, nitric acid (HNO_3), reacts with ammonia (NH_3) to form ammonium nitrate aerosols. SO_2 is oxidized in gas-phase reactions with the hydroxyl radical (OH) or in aqueous-phase reactions with O_3 or hydrogen per-
oxide (H_2O_2) to form sulfate aerosols. The sulfate and nitrate aerosols contribute to fine particulate matter pollution with aerodynamic diameters less than 2.5 μm ($PM_{2.5}$), which poses serious health concerns (Lee et al., 2015; Liu et al., 2015), degrades visibility, causes acidification of water and the biosphere with adverse effects on plants and soil, and impacts weather and climate through changes in direct radiative forcing
and indirectly modifying cloud formation and optical properties (IPCC Working Group 1 et al., 2013; Twohy, 2005). Consequently, SO_2, NO_2, and their oxidation products, O_3 and $PM_{2.5}$, are designated Criteria Pollutants (European Commission, 2015; US

Aura OMI observations of regional SO_2 and NO_2 pollution changes

N. A. Krotkov et al.

EPA, 2015). Space based characterization of these pollutants enables global consistent monitoring, which is independent from ground-based measuring networks.

The first space-based quantitative data on SO_2 mass in volcanic clouds after a major eruption (El Chichon,1982) was obtained from the six-UV band NASA's Nimbus-7 Total Ozone Mapping Spectrometer (TOMS) (Krueger, 1983). The TOMS SO_2 detection sensitivity was limited by the discrete wavelengths to exceptionally strong anthropogenic emissions, such as those produced by Norilsk smelting plants in Russia or from an accidental combustion of elemental sulfur (S) at the Al-Mishraq State Sulfur Mine Plant in Iraq (Carn et al., 2004; US Department of Veterans Affairs, 2015). Greatly improved sensitivity was demonstrated through detection of SO_2 emissions from coal-fired power plants using ESA's Global Ozone Monitoring Experiment (GOME, 1995–2005) (Burrows et al., 1997; Eisinger and Burrows, 1998) and SCanning Imaging Absorption spectrometer for Atmospheric CHartographY, (SCIAMACHY, 2002–2012) (Bovensmann et al., 1999) hyperspectral UV spectrometers. The first tropospheric NO_2 quantification was demonstrated using GOME and SCIAMACHY visible data (Leue et al., 2001; Martin et al., 2002; Richter and Burrows, 2002; Richter et al., 2005). These sensors needed several days to acquire a contiguous global map. The Ozone Monitoring Instrument (OMI) is the first satellite hyperspectral UV/Visible spectrometer with a push broom CCD detector and a wide, 2600-km swath (Levelt et al., 2006b), which enables daily, global contiguous mapping of ozone and other trace gases, including SO_2 and NO_2 (Levelt et al., 2006a). OMI was launched in July 2004 on NASA's Aura sun-synchronous afternoon equator crossing polar satellite (Schoeberl et al., 2006) and continues measurements through its 12th year, providing the longest data record currently available. OMI measurements are complemented with two GOME-2 instruments on EUMETSAT's MetOp-A (2006) and B (2012) operational polar satellites (Richter et al., 2011; Rix et al., 2012; Valks et al., 2011), although with lower spatial resolution and sensitivity to PBL sources (Fioletov et al., 2013). Next generation ESA's Sentinel series will provide higher spatial resolution and greater sensitivity to SO_2 and NO_2 sources (Ingmann et al., 2012; Veefkind et al., 2012).

In the PBL, both SO_2 and NO_2 have short lifetimes (< 1 day during the warm season) and are concentrated near their emission sources. This facilitates space-based detection of SO_2 and NO_2 sources and global characterization of their spatiotemporal variability (van der A et al., 2006, 2008; Burrows et al., 1999; Castellanos and Boersma, 2012; Eisinger and Burrows, 1998; Fioletov et al., 2013; de Foy et al., 2009; Hayn et al., 2009; He et al., 2012; Hilboll et al., 2013; Huang et al., 2013; Khokhar et al., 2005; Kim et al., 2009; Krotkov et al., 2008; Martin, 2008a; Martin et al., 2002; Mijling et al., 2009; Richter et al., 2005; Russell et al., 2012; Schneider and Van Der A, 2012; Theys et al., 2015; Valks et al., 2011; Zhou et al., 2009, 2012) and near-surface concentrations (Duncan et al., 2014; Lamsal et al., 2008, 2010, 2015; McLinden et al., 2014). Furthermore, over polluted regions satellite observable SO_2 and NO_2 vertically integrated number density profiles (columns) are highly correlated with underlying emissions, allowing space-based (i.e., "top-down") inference of spatial and temporal changes in emissions (van der A et al., 2008; Boersma et al., 2008, 2015; Carn et al., 2007; Ding et al., 2015; Duncan et al., 2013; Fioletov et al., 2011, 2015b; de Foy et al., 2014, 2015; Frost et al., 2006; Ghude et al., 2010, 2013; Hayn et al., 2009; He et al., 2012; Kim et al., 2009; Konovalov et al., 2006, 2010; Lamsal et al., 2011; Lee et al., 2011; Li et al., 2010; Lu et al., 2013, 2015; Martin, 2008b; McLinden et al., 2012, 2014; Miyazaki et al., 2012; Napelenok et al., 2008; Reuter et al., 2014; Stavrakou et al., 2008; Streets et al., 2013; Vinken et al., 2014a, b; Zhang et al., 2007), lifetime (Beirle et al., 2011; Fioletov et al., 2011, 2015b; de Foy et al., 2015; McLinden et al., 2012), physicochemical conversion (Duncan et al., 2010; Valin et al., 2013) and deposition of these species (Nowlan et al., 2014). OMI has been at the forefront of these rapid advances.

Previous OMI studies focused on specific species, emission sources and regions (van der A et al., 2008; Ahmad et al., 2007; Beirle et al., 2011; Boersma et al., 2011, 2015; Castellanos et al., 2014; Ding et al., 2015; Duncan et al., 2013; Fioletov et al., 2015b, 2011; de Foy et al., 2009, 2015; Ghude et al., 2013; Lamsal et al., 2008, 2011, 2015; Lelieveld et al., 2015; Lu et al., 2013; McLinden et al., 2014; Mebust and Cohen, 2014; Mijling and Van Der A, 2012; Mijling et al., 2009; Russell et al., 2012; Valin

et al., 2013; Vinken et al., 2014a, b; Zhou et al., 2012). While NO_2 and SO_2 are both dominated by anthropogenic emissions in polluted regions, the origin of their anthropogenic sources differs, as well as the cost and efficacy of their respective emission control techniques. The often different regional trends and abundances of NO_2 and SO_2 offer valuable insights into energy infrastructures as well as pollution control policies (Li et al., 2010; McLinden et al., 2012). In this paper we examine changes in both SO_2 and NO_2 over the world's most polluted regions during the first decade of OMI observations. Section 2 briefly summarizes OMI SO_2 and NO_2 algorithms and products. Section 3 describes regional SO_2 and NO_2 changes for the world's industrial regions with large SO_2 emissions from coal burning power plants and industries (Fig. 1). For these regions the paper provides an update to the previously published trend studies and a context for a more detailed analysis of individual sources in a companion paper in this issue (Fioletov et al., 2015a).

2   OMI standard SO_2 and NO_2 products

OMI is the result of a partnership between NASA and the Dutch and Finnish meteorological institutes and space agencies (Levelt et al., 2006b) and flies on the NASA EOS-Aura satellite (Schoeberl et al., 2006). It measures sunlight backscattered from the Earth over a wide range of Ultraviolet (UV) and visible (Vis) wavelengths to derive abundances of ozone and other trace gases important for air quality and climate. The measurements of SO_2 and NO_2 are both explicit objectives of the Aura OMI mission (Levelt et al., 2006a) that are aimed at advancing our understanding of the sources and transformation processes of these pollutants and enabling the application of OMI data to inform public policy (Streets et al., 2013). Compared with other satellite UV-Vis instruments, OMI has the highest spatial resolution, least degradation and the longest record, allowing improved space-borne estimation of NO_2 and SO_2 emissions and studying their temporal behavior (Carn et al., 2007; Castellanos and Boersma, 2012;

Duncan et al., 2013; Fioletov et al., 2011, 2013; de Foy et al., 2009; Lamsal et al., 2015; Lu et al., 2013; McLinden et al., 2012; Zhou et al., 2012).

Aura has a local equator crossing time of approximately 13:45 in the ascending node, and provides nearly global coverage each day. The OMI detector is a 2-dimensional Charge-Coupled Device (CCD) array. The instrument optics is designed such that the spatial dimension of the detector is oriented across the orbit track, with an 115° field of view, while the other dimension records spectral information. Three separate detectors (Dobber et al., 2006; Levelt et al., 2006b), designated UV-1, UV-2, and Vis, have spectral coverage (full performance) in the ranges of 270–310 nm (spectral resolution, full width at half maximum (FWHM), of 0.63 nm), 310–365 nm (0.45 nm), and 365–500 nm (0.63 nm), respectively. The OMI SO_2 product uses spectral measurements between 310.5 and 340 nm in the UV-2 (Li et al., 2013) and the NO_2 product uses spectral measurements between 405 and 465 nm in the Vis region (Boersma et al., 2011; Bucsela et al., 2013). The spatial dimension of both detectors is divided into 60 cross-track fields of view (FOV) corresponding to the specific binned CCD detector rows, such that rows 1 and 60 correspond to the western and eastern edges of the swath, respectively. Spectral measurements are made over 2 s exposure intervals. This results in along-track coverage of 13 km and cross-track coverage of 24 km for the near-nadir FOVs (CCD rows about 30). During each orbit, a total of about 1640 exposures are recorded on the sunlit side of the Earth. The width of the swath (2600 km) is such that 14–15 orbits per day are required to observe the entire surface of the Earth, although with increased FOV size at the swath edges. Beginning in 2007, some cross-track positions of the OMI swath were affected by FOV blockage and scattered light, also known as the "row anomaly" (KNMI, 2012). Here we use only unaffected OMI cross track positions (i.e., rows 6–23) throughout the entire mission, also excluding large FOVs at the edge of the swath.

2.1 Retrieval of PBL SO$_2$

OMI original PBL SO$_2$ product employed the band residual difference (BRD) algorithm, which used only 4 discrete wavelengths (Krotkov et al., 2006). The BRD product is sensitive to PBL sources, but has a high noise level (Krotkov et al., 2008) and systematic artifacts that required empirical corrections (Fioletov et al., 2011; Lee et al., 2009). In 2014 we released a new PBL SO$_2$ product, which is retrieved with a new algorithm that employs a principal component analysis (PCA) technique applied to OMI radiances (Li et al., 2013). Using a clear sky Air Mass Factor (AMF) similar to the previous SO$_2$ product, but with the full spectral content between 310.5 and 340 nm, the PCA algorithm reduces retrieval noise by a factor of two (Li et al., 2013). Recently, the Differential Optical Absorption Spectroscopy (DOAS) SO$_2$ algorithm developed for the Sentinel 5 Precursor (TROPOMI) has been applied to the OMI radiances and compared with the operational PCA product (Theys et al., 2015). The two products compare well, which lends confidence in OMI SO$_2$ data. The estimated SO$_2$ noise is similar between PCA and DOAS algorithms, when using similar assumptions for AMF calculation for pollution SO$_2$. However, the DOAS SO$_2$ algorithm requires empirical corrections to remove background bias.

In this study we will use the OMI operational PCA PBL SO$_2$ product, which contains the vertical column density (VCD) in Dobson Units (1 DU = 2.69×10^{16} molecules cm^{-2}). The product (OMSO2 v1.2.0) is publicly available from the NASA Goddard Earth Sciences (GES) Data and Information Services Center (DISC) (http://disc.sci.gsfc.nasa.gov/Aura/data-holdings/OMI/omso2_v003.shtml). The estimated 1σ noise is ~ 0.5 DU over tropical oceanic areas (Li et al., 2013). If we assume that the noise is random and that there are about 100 cloud-free samples per year, the detection limit over low latitudes can be estimated at ~ 0.2 DU for the annual mean (signal-to-noise ratio = 2 : 1 for $\pm 1\sigma$ noise). An important advantage of the PCA algorithm is that the bias over background regions (where SO$_2$ columns are below the OMI detection limit) is sufficiently small (< 0.1 DU) that it requires no empirical background correction, as applied in other

satellite SO_2 algorithms (e.g., Fioletov et al., 2013; Theys et al., 2015). The improved data quality, combined with the pixel averaging and oversampling techniques (e.g., de Foy et al., 2009; Beirle et al., 2011; Fioletov et al., 2011, 2013, 2015a, b; Lu et al., 2013; McLinden et al., 2012, 2014), provides greatly enhanced sensitivity to anthropogenic
5   SO_2 sources near the surface. It has been demonstrated that US SO_2 point sources (e.g., power plants, smelters) with emissions rates as low as ~ 30–$40\,kt\,yr^{-1}$ can be detected and analyzed using the newest OMI SO_2 product (Fioletov et al., 2015b). This limit is substantially lower than that reported ($70\,kt\,yr^{-1}$) for the previous version OMI SO_2 data (Fioletov et al., 2011).

10   2.2   Retrieval of tropospheric NO_2

There are two algorithms used operationally to determine tropospheric NO_2 VCDs: the NASA's standard product (SP, version 2.1) and the KNMI's Dutch-OMI-NO_2 (DOMINO) algorithm (TM4NO2A, version 2, http://www.temis.nl/airpollution/no2.html) (Boersma et al., 2011). Both products share a common DOAS spectral fitting of laboratory-
15   measured spectra of NO_2, H_2O, O_3, and Ring spectrum to the OMI-measured sun-normalized spectrum of backscattered radiation in the visible wavelength range of 405–465 nm to calculate NO_2 Slant Column Densities (SCDs). The estimated 1σ noise is $\sim 10^{15}$ molecules cm^{-2} or $\sim 10\,\%$ of the measured SCD over polluted regions (Boersma et al., 2011). The SCDs, after subtraction of the stratospheric contribution are con-
20   verted to tropospheric VCDs by applying AMFs, interpolated from the Look-up-Tables (LUT) with OMI-measured input parameters such as viewing geometry, climatological surface reflectivity, cloud pressure and cloud radiance fraction, assuming a priori NO_2 vertical profile shapes. The NASA and KNMI algorithms differ in how they remove the stratospheric contribution and use different a priori tropospheric NO_2 profile shapes in
25   the AMF calculation. DOMINO subtracts stratospheric SCD as determined in a data assimilation system, in which the measured SCDs are assimilated with the TM4 chemical transport model (Boersma et al., 2011). The SP estimates stratospheric NO_2 di-

rectly from OMI data without using stratospheric chemical transport models. The AMFs are calculated with a priori NO_2 monthly mean vertical profile shapes from the NASA GMI model (Bucsela et al., 2013). Despite the differences, both algorithms produce statistically similar regional trends (see Supplement Fig. S1). Here we use the SP tropospheric NO_2 VCD product version 2.1 publicly available from NASA GES DISC at http://disc.sci.gsfc.nasa.gov/Aura/data-holdings/OMI/omno2_v003.shtml. Over polluted areas the total errors in OMI tropospheric NO_2 VCDs are typically within 20 % for cloud-free FOVs, as confirmed by validation studies employing in situ and remotely sensed data (Bucsela et al., 2013; Irie et al., 2012; Lamsal et al., 2015; Oetjen et al., 2013).

2.3 Postprocessing of NO_2 and SO_2 data

For this study, level 2 (L2) tropospheric NO_2 and PBL SO_2 VCDs are gridded at different ground resolutions after excluding pixels possibly affected by the (1) row anomaly; (2) snow; (3) transient volcanic SO_2 clouds (Appendix A); (4) cloudy scenes (cloud radiance fraction > 0.5 or > 0.2 for SO_2). The standard gridded ($0.25° × 0.25°$) level 3 (L3), filtered, monthly regional mean values are used in time series analyses following Lamsal et al. (2015) (Appendix B). The L3 data are publicly available from NASA GES DISC archive at http://disc.sci.gsfc.nasa.gov/Aura/data-holdings/OMI. We also use L2 (pixel level) data oversampled at higher resolutions ($0.01° × 0.01°$ for NO_2 and $0.02° × 0.02°$ for SO_2) to create global and regional maps that highlight point pollution sources. The regional maps are created directly from pre-filtered L2 data by averaging all OMI pixels within 20 km smoothing radius (30 km for SO_2) for 3–4 year time periods. Unlike previous studies (Lee et al., 2009; Fioletov et al., 2011, 2013; Lu et al., 2013; McLinden et al., 2014), no empirical background correction was applied to the PBL SO_2 data.

3 Regional pollution changes and interpretation

Figure 1 shows SO_2 and NO_2 multi-year average maps at the beginning of the OMI mission (2005–2007) over the Northern Hemisphere. Regionally, population density (Lamsal et al., 2013), type of power generation and fuel used, economic activity, and regulatory policies determine average levels of air pollution. The SO_2 map (Fig. 1a) shows hotspots associated with major coal-fired power plants and industrial activities, such as oil and gas refining and metal smelting. The highest SO_2 is found over industrialized and populated regions in eastern China, as the world's second largest economy relies on sulfur (S) rich coal for $\sim 70\%$ of its energy consumption (Klimont et al., 2009; Zhang and Cheng, 2009). Based on bottom-up emission inventories, SO_2 emissions from China were the world's largest, at $\sim 33\,Tg\,SO_2$ in 2005 (Lu et al., 2010, 2011). High S coal-fired power plants are the major contributors to the SO_2 over the eastern US (SO_2 emissions $14.5\,Tg\,SO_2$ in 2005 (US EPA, 2014)), eastern Europe and India ($\sim 6.7\,Tg\,SO_2$ (Lu et al., 2011)). SO_2 is lower (undetectable) over the western US and western Europe where emissions of SO_2 have been relatively small due to small share of coal–fired power plants, the low S content of coal and installation of effective flue gas desulfurization devices capable of capturing more than 95% of SO_2 emissions (US EIA, 2010).

Large SO_2 column amounts are also observed over the Persian Gulf, due to emissions from the oil and gas industry in the region. Based on a bottom-up SO_2 emission inventory, the total SO_2 emissions from the Middle East in 2005 were $\sim 6\,Tg\,SO_2$ (Smith et al., 2011b), less than those from India and the US. However, OMI-observed SO_2 columns over the Persian Gulf region are significantly larger than over these two regions. This implies that real SO_2 emissions from the Middle East (particularly in the Persian Gulf) are significantly underestimated in current bottom-up emission estimates. In addition to anthropogenic SO_2, volcanic SO_2 is frequently observed over Kamchatka (Russian Federation), Japan, the South Pacific (e.g., Anatahan volcano, Mariana Islands, Mauna Loa, Hawaii), Sicily (Etna), Mexico (Popocatepetel volcano, south of

Mexico city), Central America and Montserrat, West Indies. Although transient volcanic signals were filtered from the PBL SO_2 data (Table A1), the signals from frequently erupting (e.g., Mt. Etna, Popocatepetel) or degassing volcanos remain. Except for Mt. Etna and Mt. Popocatepetl (de Foy et al., 2009), most volcanic sources are located in remote locations and do not contribute to the SO_2 in industrial regions considered here (see OMI daily SO_2 maps for the world's volcanic regions at http://so2.gsfc.nasa.gov).

The average NO_2 map (Fig. 1b) is correlated with the nighttime lights map (Fig. 1c), used here as a proxy for population density and energy production (Lamsal et al., 2013). For example, the highest NO_2 levels are observed over the world's most populated and industrialized regions including eastern China, western Europe, and the eastern US, where local NO_2 "hot spots" coincide with large urban agglomerations (Schneider et al., 2015), power plants (Duncan et al., 2013; de Foy et al., 2015) and industrial complexes. NO_2 tropospheric columns over India and the Middle East are significantly less than over China, western Europe and the US. This can be explained by low NO_x emissions, especially from mobile sources, and, partly, by year-round high temperatures, leading to shorter NO_2 lifetimes (Beirle et al., 2011). For example, Indian NO_x emissions were relatively low at 5.7 Tg NO_x in 2005 (Lu and Streets, 2012), whereas those from China and the US were 16.9 Tg NO_x (Klimont et al., 2009) and 20.4 Tg NO_x (US EPA, 2014), respectively. Relatively small, but significant areal NO_2 enhancements over west African forest are caused by seasonal biomass burning NO_x emissions (Mebust and Cohen, 2014).

The differences between the spatial distributions of NO_2 and SO_2 over the large regions indicated as boxes in Fig. 1a and b are related to economic activity, fuel types, combustion technology and different regulatory policies. The most abundant source of SO_2 is Pyrite (mostly FeS_2) and organic S in lower-grade coal as well as liquid fuel, mostly contained in heterocyclic aromatic compounds in oil, which largely accounts for high SO_2 levels over the Persian Gulf from gas flaring and oil refining. Many developed countries have regulated the S content of fuels and also required catalytic exhaust gas processing, resulting in decreased mobile-source NO_x and SO_2 emissions in exhaust.

Regulations are also focused on stack emissions of NO_x and SO_x ($SO_x = SO_2 + SO_3$) at point sources, such as power plants and smelters. This, in turn, has driven techno-logical changes upstream to meet regulatory requirements. For example, fluidized-bed combustion technology permits burning at lower temperature, producing less NO_x, and the condensed phase chemical capture of S, producing less gaseous SO_x. Chemical Loop Combustion technology uses catalytic oxygenation to oxidize the fuel largely in the absence of N_2, again resulting in greatly reduced NO_x leaving the combustion chamber. Stack scrubbers (i.e., flue gas desulfurization devices) have been widely de-ployed in Europe and the US, in particular, for existing plants, to remove SO_2 and other chemicals – notably mercury – from the flue gases, in order to meet regulatory standards. However, these changes have yet to be widely implemented in developing countries.

In addition to emissions, meteorology also plays an important role in regional air pollution, particularly on relatively short time scales (days to months). For midlatitude areas discussed in this study (the eastern US, eastern China, and eastern Europe), the concentrations of SO_2 and NO_2 often exhibit large day-to-day changes. They tend to increase under the relatively stagnant conditions ahead of a cold front and decrease dramatically after the cold front brings precipitation and strong winds into the area (Li et al., 2007). On the interannual time scale, the frequency of cold front passages may be influenced by large-scale circulation patterns such as the position of the Siberian high for eastern China (Jia et al., 2015), leading to interannual changes in SO_2 and NO_2. But meteorology probably plays a lesser role in the longer-term trends that we discuss in this study. For example, given the general trend of weakening surface winds in the Northern Hemisphere (Vautard et al., 2010), one would expect both SO_2 and NO_2 to increase over time in China, with constant emissions. While OMI did initially observe growths in both SO_2 and NO_2 over China (Sect. 3.3), the different trends be-tween the two gases after 2007 imply that different emission control measures may play a more significant role in OMI-observed trends. Similarly, the decreasing pollution levels observed over the eastern US (Sect. 3.1) and eastern Europe (Sect. 3.2) can

only be explained with a reduction in emissions. As for tropical areas such as India, the impact of year-to-year fluctuations in OMI SO_2 and NO_2 data caused by meteorological variations is small relative to the observed fast growth in emissions that occurred over areas with newly built power plants and many cities (Sect. 3.4).

5   With this understanding of the influence of different factors on anthropogenic NO_2 and SO_2 columns, we turn, in the remainder of this section, to examining regional decadal trends as seen by OMI measurements. We examine five regions indicated in Fig. 1: the eastern US, eastern Europe and Turkey, eastern China, India and the Middle East that all have SO_2 and NO_2 sources detectable by OMI. The regions are
10   in different phases of economic development and environmental regulations. We can therefore compare and contrast the trends in SO_2 and NO_2 that have different sources depending on the types of fuels burned, industrial activity and regulations. The NO_2 and SO_2 trends from these regions provide insights into underlying economic trends and pollution regulation policies.

15   **3.1   Eastern US**

Over the eastern US the highest levels of SO_2 were observed in areas of intense high-S coal combustion for industrial processes and electricity generation, including the Ohio River Valley and SW Pennsylvania (ORV, blue box in Fig. 2). Concentrations are lower (undetectable) over the western US where the local coal is intrinsically lower
20   in S and emissions of SO_2 have been relatively small (US EIA, 2010). Prior investigations involving OMI have reported a 40 % SO_2 reduction near power plants in the eastern US between 2005 and 2010 (Fioletov et al., 2011). More recent OMI observations (Fig. 2) show that the SO_2 levels continued to drop after 2010 due to both national (e.g., Clean Air Interstate Rule, CAIR (CAIR, 2009)) and state regulations. Currently,
25   US regional SO_2 levels are at or below the OMI SO_2 detection limit of ~ 0.1–0.2 DU. The dramatic decrease over the course of the first 10 years of the OMI mission (Fig. 2) closely matches trends in reported SO_2 emissions (US EPA, 2014) and sulfate deposition (-5 % yr^{-1} decrease over the eastern US from 2000–2010 (Hand et al., 2012;

Solomon et al., 2014)). This striking improvement in SO_2 coincides with implementation of control technology such as flue gas desulfurization (FGD), closure of some of the oldest coal power plants and fuel switching from coal to natural gas. Reductions in SO_2 emissions are required by the 1990 Clean Air Act Amendments (CAAA, 1990)

5　and other regulations. Substantial success has been achieved through market-based cap and trade programs such as the Acid Rain Program (ARP, 2010) and The Clean Air Interstate Rule (CAIR, 2009). These allow electricity producers to pick the most economical emission control methods. The conversion to natural gas with much less fuel S than coal has also contributed to the reduction in SO_2 pollution.

10　Unlike SO_2, which originates primarily from fuel-bound S, all high-temperature combustion, including internal combustion engines, can generate NO_x. As expected, OMI NO_2 columns peak over major cities and highways as well as over clusters of power plants. Chicago, Atlanta, and the megalopolis from Washington, DC to New York, also called the I-95 corridor (red box in Fig. 2), stand out. At the beginning of the OMI mis-

15　sion in 2005, a broad background of elevated NO_2 was detected over rural areas of the eastern US underlying the hot spots over large metropolitan areas (Fig. 2). Since that time, NO_2 has significantly decreased as a result of emission regulations on power plants and cars (Duncan et al., 2013; Lamsal et al., 2015; Lu et al., 2015; Russell et al., 2012). Decreases in NO_2 are evident in OMI NO_2 data over all major cities, especially

20　over the I-95 corridor (red box in Figs. 2 and S1) (Lu et al., 2015). NO_2 from clusters of power plants has also decreased (e.g., ORV, blue box in Fig. 2). In general, downward trends in OMI NO_2 data near US power plants correlate well with trends in NO_x emissions from the Continuous Emissions Monitoring System (CEMS) (Duncan et al., 2013) and with surface NO_2 concentrations reported by EPA Air Quality Systems (AQS)

25　(Lamsal et al., 2015; Tong et al., 2015). The NO_2 reductions are due to selective catalytic reduction (SCR) on point sources and three-way catalytic converters on vehicles (Russell et al., 2012).

Figure 3 (upper row) compares year-to-year changes in the SO_2 and NO_2 annual averages over the ORV region (blue box in Fig. 2) with other heavily polluted regions

Title Page

Abstract　Introduction

Conclusions　References

Tables　Figures

◄　►

◄　►

Back　Close

Full Screen / Esc

Printer-friendly Version

Interactive Discussion

discussed later. Overall, between 2005 and 2014 the SO_2 drop over ORV was close to 80 %, while NO_2 dropped by 40 %, the largest reductions seen in this study. The magnitude of the relative reduction in NO_2 over the I-95 corridor is similar to that over the ORV (SM: Fig. S1), suggesting similar reduction in NO_x emissions from power plants (ORV region), cities and mobile sources (I-95 region). Independent analysis of OMI NO_2 data confirmed that NO_x emissions of 35 major US urban areas decreased by ~ 50 % from 2004 to 2014 (Lu et al., 2015). We also note the faster decline in NO_2 levels before 2009 because of the installation of NO_x control devices on power plants and impact of the economic recession in 2007–2009. The annual reduction rate in NO_2 has slowed since 2009 as the US economy has recovered from the recession and the implementation of further pollution controls has slowed. As result of larger SO_2 reductions, the SO_2 / NO_2 column ratio dropped over the ORV region from its maximal values of ~ 4–5 in 2005 to less than 2 in 2014 and less than 1 over I-95 corridor (SM, Fig. S2). We expect similar change in PM speciation with increasing contribution of nitrate aerosols.

Although both SO_2 and NO_2 are Criteria Pollutants, and there remain jurisdictions in the US in violation of the National Ambient Air Quality Standards (NAAQS) for these primary pollutants, just as important is their role as precursors of key secondary air pollutants such as fine particles and ozone. The greatest numbers of Americans at risk for harmful effects of air pollution are subject to exposure to these secondary pollutants (Lee et al., 2015). Ozone is the Criteria Pollutant most likely to be found in exceedance of the US National Ambient Air Quality Standards (NAAQSs), but controlling NO_x emissions is more expensive and difficult than controlling SO_2 emissions. By 2014, total US SO_2 emissions fell to about 1/6 of their 1970 peak, but NO_x emissions only fell substantially after 2000 and are now about 1/2 of their peak in 2000 (http://www.epa.gov/ttnchie1/trends/). Because of these NO_x reductions, photochemical smog over eastern US has improved significantly over the same time period (Castellanos et al., 2011; Hogrefe et al., 2011; Simon et al., 2015). The total deposition of oxidized N (the combination of wet and dry deposition of species such as NO_2 and

Title Page

Abstract | Introduction

Conclusions | References

Tables | Figures

◀ | ▶

◀ | ▶

Back | Close

Full Screen / Esc

Printer-friendly Version

Interactive Discussion

NO$_3^-$) has improved as well (Nowlan et al., 2014) indicating that the efforts to control NO$_x$ emissions have been successful.

3.2 Eastern Europe

Europe experienced a ∼ 80 % SO$_2$ reduction between 1990 and 2011 (EEA, 2013).
Particularly, in western Europe, after significant reduction of SO$_2$ emissions in the 1980s–1990s, the SO$_2$ levels have dropped below the OMI detection limit. There are, however, detectable SO$_2$ sources in eastern Europe (Fig. 4). The spatial distribution of the observed SO$_2$ columns at the beginning of OMI mission is consistent with the spatial pattern of SO$_2$ concentrations derived from the surface monitoring stations for 2005 (Denby et al., 2010). Notable anthropogenic SO$_2$ sources include, for example, the mining and industrial districts in Donbass region in Eastern Ukraine, large coal-fired thermal power plants around the Sea of Marmara and those near Kahramanmaras in southern Turkey, as well as those near Galabovo in southeastern Bulgaria, Gorj County in southwestern Romania, Belgrade in northern Serbia, and Megalopoli in southern Greece. Most of SO$_2$ hot spots are due to use of local high S lignite (brown) coal for power generation and incomplete SO$_2$ removal from the flue gas. Figure 3 (second row) shows interannual variations in SO$_2$ and NO$_2$ columns over the Maritsa Iztok power complex in Stara Zagora, Bulgaria (see blue box in Fig. 4). Large SO$_2$ reductions (∼ 50 %) between 2011 and 2014 are consistent with the installation of desulfurization devices, while NO$_2$ remains approximately constant, suggesting stable electricity production. Another important source of SO$_2$ in the region is the Mt. Etna volcano in Sicily. OMI SO$_2$ retrievals indicate relatively constant SO$_2$ degassing from Mt. Etna during the study period, but considerable decreases in SO$_2$ over Megalopoli, Galabovo, and Gorj County, likely owing to more stringent SO$_2$ controlling measures on power plant emissions in response to mandates by the European Union. SO$_2$ emissions from Turkey, on the other hand, appear to have increased during the same period, particularly over Kahramanmaras, where new power plants went into service in 2006 (see http://globalenergyobservatory.org/geoid/42972). Increases in SO$_2$ over Serbia may re-

Title Page

Abstract | Introduction

Conclusions | References

Tables | Figures

◀ | ▶

◀ | ▶

Back | Close

Full Screen / Esc

Printer-friendly Version

Interactive Discussion

flect growth in energy consumption (mainly coal) as the country's economy recovers from wars in the 1990s.

Figure 4 (bottom row) also gives the spatial distribution of OMI tropospheric NO$_2$ over eastern Europe, which shows enhanced columns in densely populated and industrial areas. By far the largest NO$_2$ level in eastern Europe was observed over Moscow, Russian Federation (Gorchakov, 2011), followed by industrial regions in south Poland, east Germany and the Czech Republic. High columns are evident over major industrial regions of Wroclaw and large cities, such as Warsaw, Athens, and Budapest. These enhancements correlate well with emissions source distribution. While road traffic is in general the most important NO$_x$ source in Europe (EEA, 2013; Vestreng et al., 2009), in some eastern European countries the power sector is the major contributor (Zyrichidou et al., 2013). New construction and upgrades in capacity of older power plants, as well as emission control measures affect NO$_2$ columns (Castellanos and Boersma, 2012; Zhou et al., 2012). Several studies based on bottom-up emissions and satellite observations have reported substantial decreases in NO$_x$ emissions and NO$_2$ columns in most of the western European countries due to stricter emission regulations (Castellanos and Boersma, 2012; Curier et al., 2014; EEA, 2013; Lamsal et al., 2011; Schneider et al., 2015; Vestreng et al., 2009; Zhou et al., 2012). In contrast, changes in emissions are rather small in eastern Europe (Zyrichidou et al., 2010). An increase in NO$_x$ emissions is reported for those countries where implementation of the European Union (EU) air quality standards is less effective (AQ_Environment_EC, 2015; Vestreng et al., 2009). OMI measurements are consistent with previous studies, suggesting small or insignificant NO$_2$ column trends on a regional level. Changes appear to be country-specific and likely depend on the socio-economic and political situation and legislative abatement measures of the country. The EU air quality standards hold for all EU-countries (including Poland, Hungary, Bulgaria, Croatia, the Baltic States, Slovenia, Slovakia), but not for Serbia, Russia, Ukraine, Belarus, and Turkey. Some countries have asked for time extension to meet certain standards because sev-

eral Member States have particular difficulties in achieving compliance with the criteria for PM and NO_2.

3.3 Eastern China

The growth of the Chinese economy over the past two decades has been mainly driven by rapid industrialization and urbanization (Huang et al., 2013) and has been accompanied by large increases in both electricity generation (mainly coal-firedpower plants) and the number of vehicles on Chinese roads. As evident in Figs. 1a and 5, China has the world's highest SO_2 emissions, particularly over the high S coal-rich heavily industrial areas in Hebei, Henan and Shandong provinces in the North China Plain (NCP, blue box in Fig. 5) and Inner Mongolia (Li et al., 2010; Zhang et al., 2009), the highly populated Sichuan Basin (SB, red box in Fig. 5), the megacity clusters around Shanghai (the Yangtze River Delta, YRD – black box in Fig. 5) and Guangzhou–Hong Kong (the Pearl River Delta, PRD). Similarly, OMI retrievals also reveal much greater NO_2 over eastern China than other regions of the world (Fig. 1b), especially over NCP, YRD and PRD (Fig. 5). The NO_2 levels are relatively low over SB, but highest over YRD and PRD. The SO_2 / NO_2 column ratios were 8–10 over SB, 3–5 over NCP and less than 2 over YRD and PRD in 2005 (Fig. S4). The ratios reflect to some extent the level of modernization in the regions. The PRD and YRD have little industry but higher population and car density, therefore greater NO_2 relative to SO_2.

The overall SO_2 loading, although still at a relatively high level, has decreased over the years (Fig. 5). This is more clearly shown in the SO_2 time series in Fig. 3, which suggests that the SO_2 loading over the NCP peaked in 2007, and has since shown an overall decreasing trend despite relatively large year-to-year variations. The reduction in SO_2 during 2008–2010 may be attributed to both the economic recession and emission control measures before the 2008 Bejing Olympic Games (Li et al., 2010; Lu et al., 2011; Mijling et al., 2009; Witte et al., 2009). The temporary rebound in 2011 may reflect a resurgence in the economy due to stimulation by the government. This is followed by a dramatic $\sim 50\%$ reduction over the three-year period during 2012–2014

that may be attributed to both stricter emission reductions targets during the 12th Five-Year Plan (2010–2015) (Tian et al., 2013; Zhao et al., 2013), more widespread use of FGD on coal-fired power plants and industries, as well as a slowdown in the Chinese economy. We confirmed the 2012–2014 SO_2 reduction over NCP applying our SO_2 retrievals to the measurements from the new Ozone Mapping and Profiler Suite (OMPS) instrument on board NASA-NOAA Suomi National Polar Partnership (SNPP) satellite (Fig. S3). In relative terms the SO_2 reduction in 2005–2014 was larger over YRD and SB regions compared to NCP (Fig. S3).

NO_2 over NCP, on the other hand, peaked in 2011 after dramatic $\sim 50\%$ increase since 2009 (Fig. 3) and decreased slightly in 2012 and 2013 (Fig. 3). Temporary drop in 2008 can be attributed to strict pollution reduction measures implemented before 2008 Olympic games and economic recession. The reductions were strongest in Beijing, Tianjin and Schijiazhuang regions (Mijling et al., 2009; Witte et al., 2009). The dramatic drop in NO_2 in 2014 is likely a result of the slowest economic growth rate for China in nearly 25 years. According to the National Bureau of Statistics, the electricity generation by thermal power plants decreased by several percent in the second half of the year as compared with 2013. Similarly there is also a slowdown in coal-intensive industrial sectors (Guay, 2015) and stricter emission control policies (MEP, 2013). Independent satellite NO_2 retrievals with GOME-2A, GOME-2B and OMI also confirm large reduction in NO_2 over eastern China between 2013 and 2014 (Richter et al., 2015). Over SB and YRD NO_2 columns peaked in 2010 and remained realatively constant afterwards (Fig. S1). As a result of the different trends between SO_2 and NO_2 the SO_2 to NO_2 ratios dropped to their lowest values ~ 2–3, ~ 1–2 and less than one over SB, NCP and YRD regions, respectively (Fig. S4).

3.4 India

Figure 6 shows multi-year mean OMI SO_2 and NO_2 maps over India. A number of SO_2 and NO_2 hot spots are observed, and they match the locations of large coal-fired power plants and major cities (Ghude et al., 2011, 2013). This is because coal-fired

power plants are the dominant SO_2 and NO_x emission sources in India, and they are often built near large cities where other anthropogenic emissions are also high. Figure 6 also shows that from 2005 to 2014, there was an increase in the OMI-observed SO_2 and NO_2 columns over India, mainly reflecting the fast expansion of the power sector

5 driven by rapid economic growth. Based on an updated unit-based coal-fired power sector database (Lu and Streets, 2012; Lu et al., 2013), the total installed capacity, power generation, and fuel consumption of Indian coal-fired power plants increased dramatically by 126, 91, and 93 %, respectively, during 2005–2014. The SO_2 emissions from power plants are high, because S in local coal is mostly in organic form and cannot

10 be removed by physical cleaning methods (Lookman and Rubin, 1998).

Unlike the US, Europe, and China, SO_2 and NO_x emitted from coal-fired power plants are not regulated in India and the installation and operation rates of SO_2 and NO_x emission control devices are very low. FGD devices for SO_2 were reported to be operating in only three power plants at the beginning of OMI mission (Chikkatur

15 et al., 2007). As for NO_x emissions, they are also not regulated in India for coal-fired power plants. Although some new plants were reported to be equipped with low-NO_x burners (LNB), the actual installation rate and performance of these LNB devices are not known. Based on bottom-up emission inventories we estimate that SO_2 and NO_x emissions from Indian coal-fired power plants increased by 103 and 94 %, respectively,

20 during 2005–2014 (Lu and Streets, 2012; Lu et al., 2013). As shown in Fig. 3, the growth rates in OMI-observed SO_2 (200 ± 50 %) and NO_2 (50 ± 20 %) columns during 2005–2014 were particularly large over the industrial regions in Chhattisgarh and Odisha (blue box in Fig. 6), one of India's most active areas in terms of building new power plants.

25 By the end of 2014, the total installed capacity of coal-fired power plants in this region was 28 GW, 85 % of which (~ 24 GW) was installed after 2005, accounting for ~ 26 % of the total newly installed capacity in India. As a result, SO_2 and NO_x emissions from coal-fired power plants in this region were estimated to increase both by ~ 190 % from 2005 to 2014 (Lu and Streets, 2012; Lu et al., 2013), largely in line with OMI

observations (Fig. 3). India's total annual SO_2 emissions almost doubled from 6.7 Tg in 2005 to estimated 12 Tg in 2014. In 2014, India has not only surpassed the US to be the world's second largest SO_2 emitting country, but also has reached more than 40 % of the SO_2 emissions of the world's largest emitter, China.

3.5 Middle East

In the Middle East, abundant oil and gas deposits supply cheap and relatively clean fuels for electricity generation, water desalination, and industries. OMI detects the largest SO_2 emissions over the Persian Gulf. The sources for these emissions are apparently not included in the current global emission inventory such as the 2008 EDGAR-HTAP dataset (e.g., http://edgar.jrc.ec.europa.eu/edgar_album/v42/SO2/TOTALS/v42_SO2_2008_TOT.jpg). Based on the most recent SO_2 emission inventory, the total SO_2 emissions from the Middle East in 2005 were $\sim$ 6 Tg (Klimont et al., 2013; Smith et al., 2011a), less than those from India and the US. However, OMI observed SO_2 columns over the Gulf region are significantly larger than those over India and US. That suggests that the real SO_2 emissions from the Middle East (particularly in the Persian Gulf) may be several times higher than current bottom-up emission estimates. This is consistent with independent OMI SO_2 retrievals (Theys et al., 2015). Inverse modeling using OMI and SCIAMACHY retrievals also suggests an underestimate of SO_2 emissions from the Persian Gulf (Lee et al., 2011).

In-situ measurements of SO_2 and other pollutants are rarely reported for the region, but available data generally indicate significant SO_2 loading over the Persian Gulf. For example, an aircraft campaign conducted north of the United Arab Emirates during winter 2001 measured SO_2 concentrations of up to 40 ppb (see https://www.rap.ucar.edu/asr2002/i-precip_physics/precip_physics.htm), greater than what has been previously observed over eastern China (Dickerson et al., 2007; He et al., 2012). The largest hotspot observed by the aircraft, near Zirku Island, also appears to be co-located with a hotspot in OMI retrievals. In another study, passive sampling of SO_2 at various locations on Khark Island near the north end of the Gulf during 2003–

2004 reported that the SO_2 loading was above the air quality standard (sometimes by several-fold) most of the time (Pourzamani et al., 2012). These high SO_2 columns over the Persian Gulf are likely the result of gas flaring activities from offshore oil and natural gas facilities, although shipping emissions and other sources may also contribute to them. Gas flaring is used on offshore oil rigs to dispose of gases such as hydrogen sulfide (H_2S) for safety, operational, and economic reasons and can have significant impacts on the local and regional environment in the Middle East.

Middle East cities also show SO_2 emissions due to both mobile and stationary sources. Oil-burning boilers may constitute another important source of SO_2 in cities or population centers, as implied by the relatively high sulfate ($\sim 10\,\mu g\,m^{-3}$) that is closely associated with oil combustion tracers (e.g., vanadium), according to an aerosol source apportionment study for Kuwait City (Alolayan et al., 2013). The S content in gasoline and diesel is much higher in this region as compared with others such as Europe, which enforces stricter emission control measures (see http://www.unep.org/transport/pcfv/PDF/JordanWrkshp-MiddleEastFuelQuality.pdf). Some of the largest point SO_2 sources in the region coincide with smelters or oil refineries, such as the Sarcheshmeh Copper Complex in Kerman Province, Iran, which is the largest copper smelter in the Middle East. Figure 3 (bottom row) show interannual variations in observed SO_2 and NO_2 columns over Persian Gulf (blue box in Fig. 7). Since 2010 SO_2 columns have steadily dropped by $\sim 20\,\%$, but increased again in 2014 to 2005 levels (but still less than 2010 levels). A recent study (Lelieveld et al., 2015) reported that OMI SO_2 over Persian Gulf increased between 2005 and 2010, and then decreased between 2010 and 2014. Their results are based on retrievals using a different algorithm, but are qualitatively consistent with this study.

OMI retrieved regional NO_2 levels over Middle East are much smaller than over China (Fig. 6) and the US (Fig. 2). This may also be the results of the short lifetime of NO_2 in this hot and photochemically active region (Beirle et al., 2011). NO_x emissions in the region are associated with power generation and mobile sources. Local NO_2 enhancements coincide with heavily populated cities that have high car densities, such

as Jerusalem (Israel) and Cairo (Egypt) (Boersma et al., 2009), Tehran (Iran), Kuwait City (Kuwait), Dubai (UAE), Riyadh and Jeddah (Saudi Arabia). In terms of regional trend over the Persian Gulf (blue box in Fig. 7), NO_2 columns increased by $\sim 20\%$ between 2005 and 2008, but remained approximately constant afterwards (Fig. 3). For major metropolitan areas in the region, Lelieveld et al. (2015) focused on the reversal of OMI NO_2 trends due to recent air quality regulations and domestic and international conflicts in the region. Their results are, for the most part, qualitatively consistent with Fig. 7. For example, their reported decrease of NO_2 over Damascus, Syria since 2011 (due to civil war) and increase over Baghdad, Iraq since 2007 are also visible in Fig. 7.

4   Conclusions

The first decade of OMI observations (2005–2014) have yielded profound insights into the spatial distribution and temporal trends in SO_2 and NO_2 around the world. For regions with detailed bottom-up emissions estimates or continuous emissions monitoring, OMI shows generally good agreement with these independent data sources. OMI-derived trends also agree well with those from available in situ measurements and deposition data. This adds confidence to the use of OMI to track locations, changes, and transport patterns of SO_2 and NO_2 over areas of the planet lacking local observations. In many regions pollution levels have changed dramatically reflecting underlying changes in SO_2 and NO_x emissions (Fig. 8): (1) over the eastern US, both NO_2 and SO_2 levels decreased dramatically from 2005 to 2014. SO_2 concentrations over the Ohio River Valley and western Pennsylvania fell by 80 %, consistent with the National Emission Inventory (NEI), which reports a decrease of about 66 % for total US emissions. NO_2 concentrations over the eastern US fell by more than 40 %, also consistent with the NEI trend for emissions from the entire country. The Clean Air Act Amendments and regulations such as CAIR mandated these emissions reductions, and OMI confirmed their efficacy. (2) Over eastern Europe, OMI observed substantial (more than 50 %) SO_2 decreases in the vicinity of the largest coal-fired power plants, where FGD

was installed during the study period. Over some areas including Turkey and Serbia, local SO_2 increased, perhaps because of increased industrial activity. NO_2 levels in the vicinity of the largest eastern European power plants in Bulgaria remain constant. (3) Over China, highest SO_2 and NO_2 levels are observed over the North China Plain, with the highest concentrations in the world. SO_2 peaked in 2007, with a secondary peak in 2011, but by 2014 SO_2 has fallen to half of the levels seen at the beginning of the OMI record in 2005. Total Chinese electricity production and coal combustion have increased during the same period, and the observed decrease likely has resulted from centralization of industry and power production and the implementation of pollution control devices. NO_2 concentrations peaked in 2011, but by 2014 have returned to 2005 levels. (4) Over India, despite relatively low levels as compared with China, both SO_2 and NO_2 have increased, particularly over the northeast where a large number of newly built coal power plants have doubled SO_2 while increasing NO_2 by $\sim 50\,\%$. This is the fastest increase in pollution concentrations observed by OMI. In 2014 India has surpassed the US to become the world's second largest SO_2 emitting country. (5) Over the Middle East, OMI detected several SO_2 hot spots with a broad maximum over the Persian Gulf region. These hotspots are probably related to oil and gas operations but are mostly absent in bottom-up emission inventories, such as EDGAR. High concentrations of NO_2 are observed over major cities but less so over oil and gas operations. SO_2 shows no discernable trend over the Gulf while NO_2 rose from 2005 to 2008 and has since remained largely unchanged.

In summary, this study demonstrates that satellite remote sensing from advanced instruments such as OMI can provide long-term, nearly continuous global monitoring of SO_2 and NO_2. Where in situ concentration measurements, emission inventories, and deposition monitoring are available, OMI provides complementary measurements to supplement and verify those other data sources. It can also find unreported or underreported major emissions such as over the Persian Gulf. OMI SO_2 and NO_2 data can also help to further our understanding of the production and impact of secondary pollutants such as tropospheric ozone and particulate matter.

Space-based monitoring plays an increasingly important role in the science of tropospheric chemistry and air quality applications to help mitigate anthropogenic and natural impacts on climate, sensitive ecosystems, and human health. It is essential to continue and maintain overlapping long-term satellite data records. The baseline established during the first 10 years of OMI is invaluable for the interpretation of measurements from future satellite atmospheric chemistry missions. The OMI NO_2 and SO_2 data sets used in this study will be continued by the TROPOspheric Monitoring Instrument (TROPOMI) (Veefkind et al., 2012), which is planned for launch on ESA's Sentinel 5 Precursor satellite in 2016. TROPOMI will have a significantly higher signal-to-noise and spatial resolution (7 km × 7 km at nadir) than OMI (13 km × 24 km at nadir); both features are very important for monitoring point pollution sources and trends. TROPOMI is part of the European Sentinel series that will continue the global pollution data record for another 20 years (Ingmann et al., 2012). The space-based capabilities for air quality applications will be further enhanced by the addition of high-ground resolution (at 4 km by 4 km at nadir) hourly observations from the three geostationary satellites over North America (TEMPO, http://tempo.si.edu), over Europe (Sentinel 4 UVN (Ingmann et al., 2012)) and East Asia (GEMS). This constellation will allow for unprecedented observations of the key pollutants in the atmosphere.

Appendix A: Filtering transient volcanic clouds

Days affected by transient volcanic SO_2 signals were excluded as follows. Every day the region-wide 99.9-percentile of SO_2 VCDs was computed. If it was found to exceed a threshold value (Table A1) then all data from that day were excluded. This was found to perform better than a simple maximum SO_2 or NO_2 column cut-off as it tended to remove volcanic signals that, while elevated, would not exceed the maximum. A disadvantage of this method is that, while the volcanic contamination would generally only impact a small portion of the region, all data from that day were removed. The SO_2 threshold employed varied from 5 to 10 DU (Table A1) and was chosen by examining

the 99.9-percentile time series during known periods of minimal volcanic activity. Different regions were found to be affected differently, a result of their proximity to significant eruptions. For regions that span the northern mid-latitudes such as US, Europe, and China, many of the days occurred in 2008 and 2009 and can be attributed to the eruptions of Kasatochi (Aleutian Islands, Alaska, August 2008, 52° N) and Sarychev (Kuril Islands, eastern Russia, June 2009, 48° N). By contrast, the Nabro eruption (northern Africa, June 2011, 13.37° N) removed the most days over India and Africa whereas the Middle East appeared to be largely unaffected by volcanic emissions.

Appendix B: Timeseries analysis

We use standard Level 3 monthly regional mean SO_2 and NO_2 columns and a regression model discussed in Lamsal et al. (2015) to compare inter-annual timeseries for different regions. The time series of monthly average values (Ω) are assumed to be comprised of three additive subcomponents: a seasonal component (α), a linear trend component (β), and residues or noise (R) component:

$$\Omega(t) = \alpha(t) + \beta t + R(t) \tag{B1}$$

where, t represents time (month). The time dependent seasonal regression coefficient (α) is given by a constant plus intra-annual sine and cosine harmonic series (Randel and Cobb, 1994):

$$\alpha(t) = c_0 + \sum_{j=1}^{3} \left(c_{1j} \sin\left(\frac{2\pi j t}{12}\right) + c_{2j} \cos\left(\frac{2\pi j t}{12}\right) \right), \tag{B2}$$

where c_0, c_{1j}, and c_{2j} are constant coefficients. The major portion of the annual cycle is explained by the seasonal variation of the NO_x and SO_2 lifetime. Other factors, such as monthly variation in source strength, could also affect the annual variation of NO_2 and SO_2 columns, but these contributions especially for NO_2 to the seasonal cycle are

Aura OMI observations of regional SO₂ and NO₂ pollution changes

N. A. Krotkov et al.

Title Page

Abstract	Introduction
Conclusions	References
Tables	Figures

|◄ | ►|

◄ | ►

Back | Close

Full Screen / Esc

Printer-friendly Version

Interactive Discussion

typically smaller especially for polluted areas. The seasonal pattern can evolve with time. We identify and extract seasonal and trend components by exploiting changes in the seasonal pattern (amplitude and phase) for individual years. For each year we fit a regression line using monthly observations from that year itself and 6 observations each from adjacent years. This provides a series of local regression lines that incorporate explicit time dependence. Comparison of local regression lines with high- and low-amplitude regression lines allows identification and isolation of two seasonal terms (α_1, α_2, where $\alpha = \alpha_1 + \alpha_2$ in Eq. 1) and the linear trend (β) and residues. Since we are interested in interannual changes, we do not explicitly derive linear trend, but rather calculate changes from 2005 from de-seasonalized NO_2 and SO_2 columns (Fig. 3).

The Supplement related to this article is available online at doi:10.5194/acpd-15-26555-2015-supplement.

References

Ahmad, Z., McClain, C. R., Herman, J. R., Franz, B. A., Kwiatkowska, E. J., Robinson, W. D., Bucsela, E. J., and Tzortziou, M.: Atmospheric correction for NO_2 absorption in retrieving water-leaving reflectances from the SeaWiFS and MODIS measurements, Appl. Optics, 46, 6504–6512, doi:10.1364/AO.46.006504, 2007.

Alolayan, M. A., Brown, K. W., Evans, J. S., Bouhamra, W. S., and Koutrakis, P.: Source apportionment of fine particles in Kuwait City, Sci. Total Environ., 448, 14–25, doi:10.1016/j.scitotenv.2012.11.090, 2013.

AQ_Environment_EC: Air Quality – Environment – European Commission, available at: http://ec.europa.eu/environment/air/quality/legislation/time_extensions.htm (last access: 18 August 2015), 2015.

ARP: Acid Rain Program, Clean Air Markets, US Environmental Protection Agency, EPA, available at: http://www.epa.gov/airmarkets/programs/arp/ (last access: 9 August 2015), 2010.

Beirle, S., Boersma, K. F., Platt, U., Lawrence, M. G., and Wagner, T.: Megacity emissions and lifetimes of nitrogen oxides probed from space, Science, 333, 1737–1739, doi:10.1126/science.1207824, 2011.

Boersma, K. F., Jacob, D. J., Eskes, H. J., Pinder, R. W., Wang, J., and van der A, R. J.: Intercomparison of SCIAMACHY and OMI tropospheric NO_2 columns: Observing the diurnal evolution of chemistry and emissions from space, J. Geophys. Res.-Atmos., 113, D16S26, doi:10.1029/2007JD008816, 2008.

Boersma, K. F., Jacob, D. J., Trainic, M., Rudich, Y., DeSmedt, I., Dirksen, R., and Eskes, H. J.: Validation of urban NO_2 concentrations and their diurnal and seasonal variations observed from the SCIAMACHY and OMI sensors using in situ surface measurements in Israeli cities, Atmos. Chem. Phys., 9, 3867–3879, doi:10.5194/acp-9-3867-2009, 2009.

Boersma, K. F., Eskes, H. J., Dirksen, R. J., van der A, R. J., Veefkind, J. P., Stammes, P., Huijnen, V., Kleipool, Q. L., Sneep, M., Claas, J., Leitão, J., Richter, A., Zhou, Y., and Brunner, D.: An improved tropospheric NO_2 column retrieval algorithm for the Ozone Monitoring Instrument, Atmos. Meas. Tech., 4, 1905–1928, doi:10.5194/amt-4-1905-2011, 2011.

Boersma, K. F., Vinken, G. C. M., and Tournadre, J.: Ships going slow in reducing their NO_x emissions: changes in 2005–2012 ship exhaust inferred from satellite measurements over Europe, Environ. Res. Lett., 10, 074007, doi:10.1088/1748-9326/10/7/074007, 2015.

Bovensmann, H., Burrows, J. P., Buchwitz, M., Frerick, J., Noël, S., Rozanov, V. V., Chance, K. V., and Goede, A. P. H.: SCIAMACHY: mission objectives and measurement modes, J. Atmos. Sci., 56, 127–150, doi:10.1175/1520-0469(1999)056<0127:SMOAMM>2.0.CO;2, 1999.

Bucsela, E. J., Krotkov, N. A., Celarier, E. A., Lamsal, L. N., Swartz, W. H., Bhartia, P. K., Boersma, K. F., Veefkind, J. P., Gleason, J. F., and Pickering, K. E.: A new stratospheric and

Title Page

Abstract | Introduction

Conclusions | References

Tables | Figures

|◄ | ►|

◄ | ►

Back | Close

Full Screen / Esc

Printer-friendly Version

Interactive Discussion

tropospheric NO$_2$ retrieval algorithm for nadir-viewing satellite instruments: applications to OMI, Atmos. Meas. Tech., 6, 2607–2626, doi:10.5194/amt-6-2607-2013, 2013.

Burrows, J. P., Buchwitz, M., Rozanov, V., Weber, M., Richter, A., Ladstätter-Weißenmayer, A., and Eisinger, M.: The Global Ozone Monitoring Experiment (GOME): Mission, Instrument Concept, and First Scientific Results, Eur. Sp. Agency, Special Publ. ESA SP, 414 PART 2, 585–590, doi:10.1175/1520-0469(1999)056<0151:TGOMEG>2.0.CO;2, 1997.

Burrows, J. P., Weber, M., Buchwitz, M., Rozanov, V., and Ladst, A.: The Global Ozone Monitoring Experiment (GOME): mission concept and first scientific results, J. Atmos. Sci., 56, 151–175, 1999.

CAAA: EPA History: Clean Air Act Amendments of 1990, available at: http://www2.epa.gov/aboutepa/epa-history-clean-air-act-amendments-1990 (last access: 9 August 2015), 1990.

CAIR: Programs, Clean Air Markets, US Environmental Protection Agency, available at: http://www.epa.gov/airmarkets/programs/index.html (last access: 9 August 2015), 2009.

Carn, S. A., Krueger, A. J., Krotkov, N. A., and Gray, M. A.: Fire at Iraqi sulfur plant emits SO$_2$ clouds detected by Earth Probe TOMS, Geophys. Res. Lett., 31, 2–5, doi:10.1029/2004GL020719, 2004.

Carn, S. A., Krueger, A. J., Krotkov, N. A., Yang, K., and Levelt, P. F.: Sulfur dioxide emissions from Peruvian copper smelters detected by the Ozone Monitoring Instrument, Geophys. Res. Lett., 34, L09801, doi:10.1029/2006GL029020, 2007.

Castellanos, P. and Boersma, K. F.: Reductions in nitrogen oxides over Europe driven by environmental policy and economic recession, Sci. Rep., 2, 265, doi:10.1038/srep00265, 2012.

Castellanos, P., Marufu, L. T., Doddridge, B. G., Taubman, B. F., Schwab, J. J., Hains, J. C., Ehrman, S. H., and Dickerson, R. R.: Ozone, oxides of nitrogen, and carbon monoxide during pollution events over the eastern United States: an evaluation of emissions and vertical mixing, J. Geophys. Res., 116, D16307, doi:10.1029/2010JD014540, 2011.

Castellanos, P., Boersma, K. F., and van der Werf, G. R.: Satellite observations indicate substantial spatiotemporal variability in biomass burning NO$_x$ emission factors for South America, Atmos. Chem. Phys., 14, 3929–3943, doi:10.5194/acp-14-3929-2014, 2014.

Curier, R. L., Kranenburg, R., Segers, A. J. S., Timmermans, R. M. A., and Schaap, M.: Synergistic use of OMI NO$_2$ tropospheric columns and LOTOS–EUROS to evaluate the NO$_x$ emission trends across Europe, Remote Sens. Environ., 149, 58–69, doi:10.1016/j.rse.2014.03.032, 2014.

Aura OMI observations of regional SO$_2$ and NO$_2$ pollution changes

N. A. Krotkov et al.

Title Page

Abstract | Introduction

Conclusions | References

Tables | Figures

◀ | ▶

◀ | ▶

Back | Close

Full Screen / Esc

Printer-friendly Version

Interactive Discussion

Denby, B., Sundvor, I., Cassiani, M., de Smet, P., de Leeuw, F., and Horálek, J.: Spatial mapping of ozone and SO_2 trends in Europe, Sci. Total Environ., 408, 4795–4806, doi:10.1016/j.scitotenv.2010.06.021, 2010.

Dickerson, R. R., Li, C., Li, Z., Marufu, L. T., Stehr, J. W., McClure, B., Krotkov, N., Chen, H., Wang, P., Xia, X., Ban, X., Gong, F., Yuan, J., and Yang, J.: Aircraft observations of dust and pollutants over northeast China: insight into the meteorological mechanisms of transport, J. Geophys. Res.-Atmos., 112, 1–13, doi:10.1029/2007JD008999, 2007.

Ding, J., van der A, R. J., Mijling, B., Levelt, P. F., and Hao, N.: NO_x emission estimates during the 2014 Youth Olympic Games in Nanjing, Atmos. Chem. Phys., 15, 9399–9412, doi:10.5194/acp-15-9399-2015, 2015.

Dobber, M. R., Dirksen, R. J., Levelt, P. F., Van Den Oord, G. H. J., Voors, R. H. M., Kleipool, Q., Jaross, G., Kowalewski, M., Hilsenrath, E., Leppelmeier, G. W., de Vries, J. D. V. J., Dierssen, W., and Rozemeijer, N. C.: Ozone monitoring instrument calibration, IEEE T. Geosci. Remote, 44, 1209–1238, doi:10.1109/TGRS.2006.869987, 2006.

Duncan, B. N., Yoshida, Y., Olson, J. R., Sillman, S., Martin, R. V., Lamsal, L., Hu, Y., Pickering, K. E., Retscher, C., Allen, D. J., and Crawford, J. H.: Application of OMI observations to a space-based indicator of NO_x and VOC controls on surface ozone formation, Atmos. Environ., 44, 2213–2223, doi:10.1016/j.atmosenv.2010.03.010, 2010.

Duncan, B. N., Yoshida, Y., de Foy, B., Lamsal, L. N., Streets, D. G., Lu, Z., Pickering, K. E., and Krotkov, N. A.: The observed response of Ozone Monitoring Instrument (OMI) NO_2 columns to NO_x emission controls on power plants in the United States: 2005–2011, Atmos. Environ., 81, 102–111, doi:10.1016/j.atmosenv.2013.08.068, 2013.

Duncan, B. N., Prados, A. I., Lamsal, L. N., Liu, Y., Streets, D. G., Gupta, P., Hilsenrath, E., Kahn, R. A., Nielsen, J. E., Beyersdorf, A. J., Burton, S. P., Fiore, A. M., Fishman, J., Henze, D. K., Hostetler, C. A., Krotkov, N. A., Lee, P., Lin, M., Pawson, S., Pfister, G., Pickering, K. E., Pierce, R. B., Yoshida, Y., and Ziemba, L. D.: Satellite data of atmospheric pollution for US air quality applications: examples of applications, summary of data end-user resources, answers to FAQs, and common mistakes to avoid, Atmos. Environ., 94, 647–662, doi:10.1016/j.atmosenv.2014.05.061, 2014.

EEA: European Union Emission Inventory Report 1990–2011 Under the UNECE Convention on Long-range Transboundary Air Pollution (LRTAP), European Environment Agency (EEA), Technical report No 10/2013, doi:10.2800/44480, 2013.

Title Page

Abstract | Introduction

Conclusions | References

Tables | Figures

|◄ | ►|

◄ | ►

Back | Close

Full Screen / Esc

Printer-friendly Version

Interactive Discussion

Eisinger, M. and Burrows, J. P.: Tropospheric sulfur dioxide observed by the ERS-2 GOME instrument, Geophys. Res. Lett., 25, 4177–4180, doi:10.1029/1998GL900128, 1998.

EPA: Reactive Nitrogen in the United States: An Analysis of Inputs, Flows, Consequences, and Management Options, Washington, DC, available at: http://yosemite.epa.gov/sab/sabproduct.nsf/WebBOARD/INCFullReport/$File/FinalINCReport_8_19_11(withoutsignatures).pdf (last access: 12 July 2015), 2011.

EPA: Integrated Science Assessment of Ozone and Related Photochemical Oxidants, available at: http://cfpub.epa.gov/ncea/isa/recordisplay.cfm?deid=247492#Download (last access: 12 July 2015), 2013.

European Commission: Air Quality Standards – Environment – European Commission, available at: http://ec.europa.eu/environment/air/quality/standards.htm (last access: 5 August 2015), 2015.

Fioletov, V. E., McLinden, C. A., Krotkov, N., Moran, M. D., and Yang, K.: Estimation of SO_2 emissions using OMI retrievals, Geophys. Res. Lett., 38, L21811, doi:10.1029/2011GL049402, 2011.

Fioletov, V. E., McLinden, C. A., Krotkov, N., Yang, K., Loyola, D. G., Valks, P., Theys, N., Van Roozendael, M., Nowlan, C. R., Chance, K., Liu, X., Lee, C., and Martin, R. V.: Application of OMI, SCIAMACHY, and GOME-2 satellite SO_2 retrievals for detection of large emission sources, J. Geophys. Res.-Atmos., 118, 11399–11418, doi:10.1002/jgrd.50826, 2013.

Fioletov, V. E., McLinden, C., Krotkov, N. A., and Li, C.: A global catalogue of SO_2 sources and emissions derived from Ozone Monitoring Instrument, Atmos. Chem. Phys. Discuss., in preparation, 2015a.

Fioletov, V. E., McLinden, C. A., Krotkov, N., and Li, C.: Lifetimes and emissions of SO_2 from point sources estimated from OMI, Geophys. Res. Lett., 42, 1969–1976, doi:10.1002/2015GL063148, 2015b.

de Foy, B., Krotkov, N. A., Bei, N., Herndon, S. C., Huey, L. G., Martínez, A.-P., Ruiz-Suárez, L. G., Wood, E. C., Zavala, M., and Molina, L. T.: Hit from both sides: tracking industrial and volcanic plumes in Mexico City with surface measurements and OMI SO_2 retrievals during the MILAGRO field campaign, Atmos. Chem. Phys., 9, 9599–9617, doi:10.5194/acp-9-9599-2009, 2009.

De Foy, B., Wilkins, J. L., Lu, Z., Streets, D. G., and Duncan, B. N.: Model evaluation of methods for estimating surface emissions and chemical lifetimes from satellite data, Atmos. Environ., 98, 66–77, doi:10.1016/j.atmosenv.2014.08.051, 2014.

Title Page

Abstract | Introduction

Conclusions | References

Tables | Figures

|◀ | ▶|

◀ | ▶

Back | Close

Full Screen / Esc

Printer-friendly Version

Interactive Discussion

De Foy, B., Lu, Z., Streets, D. G., Lamsal, L. N., and Duncan, B. N.: Estimates of power plant NO_x emissions and lifetimes from OMI NO_2 satellite retrievals, Atmos. Environ., 116, 1–11, doi:10.1016/j.atmosenv.2015.05.056, 2015.

Frost, G. J., McKeen, S. A., Trainer, M., Ryerson, T. B., Neuman, J. A., Roberts, J. M., Swanson, A., Holloway, J. S., Sueper, D. T., Fortin, T., Parrish, D. D., Fehsenfeld, F. C., Flocke, F., Peckham, S. E., Grell, G. A., Kowal, D., Cartwright, J., Auerbach, N., and Habermann, T.: Effects of changing power plant NO_x emissions on ozone in the eastern United States: proof of concept, J. Geophys. Res., 111, D12306, doi:10.1029/2005JD006354, 2006.

Galloway, J. N., Leach, A. M., Bleeker, A., and Erisman, J. W.: A chronology of human understanding of the nitrogen cycle, Philos. T. R. Soc. Lond., 368, doi:10.1098/rstb.2013.0120, 2013.

Ghude, S. D., Lal, D. M., Beig, G., Van Der A, R., and Sable, D.: Rain-induced soil NO_x emission from India during the onset of the summer monsoon: a satellite perspective, J. Geophys. Res.-Atmos., 115, D16304, doi:10.1029/2009JD013367, 2010.

Ghude, S. D., Kulkarni, P. S., Kulkarni, S. H., Fadnavis, S., and Van Der A, R. J.: Temporal variation of urban NO_x concentration in India during the past decade as observed from space, Int. J. Remote Sens., 32, 849–861, doi:10.1080/01431161.2010.517797, 2011.

Ghude, S. D., Pfister, G. G., Jena, C., Van Der A, R. J., Emmons, L. K., and Kumar, R.: Satellite constraints of nitrogen oxide (NO_x) emissions from India based on OMI observations and WRF-Chem simulations, Geophys. Res. Lett., 40, 423–428, doi:10.1029/2012GL053926, 2013.

Gorchakov, G., Semoutnikova, E., Karpov, A., and Lezina, E.: Air Pollution in Moscow Megacity, Chapter 11, in: Advanced Topics in Environmental Health and Air Pollution Case Studies, edited by: Moldoveanu, A. M., InTech., 2011.

Guay, J.: China's thirst for coal is drying up, available at: http://www.huffingtonpost.com/justin-guay/chinas-thirst-for-coal-is_b_5358194.html (last access: 26 August 2015), 2015.

Hand, J. L., Schichtel, B. A., Malm, W. C., and Pitchford, M. L.: Particulate sulfate ion concentration and SO_2 emission trends in the United States from the early 1990s through 2010, Atmos. Chem. Phys., 12, 10353–10365, doi:10.5194/acp-12-10353-2012, 2012.

Hayn, M., Beirle, S., Hamprecht, F. A., Platt, U., Menze, B. H., and Wagner, T.: Analysing spatio-temporal patterns of the global NO_2-distribution retrieved from GOME satellite observations using a generalized additive model, Atmos. Chem. Phys., 9, 6459–6477, doi:10.5194/acp-9-6459-2009, 2009.

Title Page

Abstract | Introduction

Conclusions | References

Tables | Figures

|◄ | ►|

◄ | ►

Back | Close

Full Screen / Esc

Printer-friendly Version

Interactive Discussion

He, H., Li, C., Loughner, C. P., Li, Z., Krotkov, N. A., Yang, K., Wang, L., Zheng, Y., Bao, X., Zhao, G., and Dickerson, R. R.: SO_2 over central China?: measurements, numerical simulations and the tropospheric sulfur budget, J. Geophys. Res.-Atmos., 117, 1–15, doi:10.1029/2011JD016473, 2012.

Hilboll, A., Richter, A., and Burrows, J. P.: Long-term changes of tropospheric NO_2 over megacities derived from multiple satellite instruments, Atmos. Chem. Phys., 13, 4145–4169, doi:10.5194/acp-13-4145-2013, 2013.

Hogrefe, C., Hao, W., Zalewsky, E. E., Ku, J.-Y., Lynn, B., Rosenzweig, C., Schultz, M. G., Rast, S., Newchurch, M. J., Wang, L., Kinney, P. L., and Sistla, G.: An analysis of long-term regional-scale ozone simulations over the Northeastern United States: variability and trends, Atmos. Chem. Phys., 11, 567–582, doi:10.5194/acp-11-567-2011, 2011.

Huang, J., Zhou, C., Lee, X., Bao, Y., Zhao, X., Fung, J., Richter, A., Liu, X., and Zheng, Y.: The effects of rapid urbanization on the levels in tropospheric nitrogen dioxide and ozone over East China, Atmos. Environ., 77, 558–567, doi:10.1016/j.atmosenv.2013.05.030, 2013.

Ingmann, P., Veihelmann, B., Langen, J., Lamarre, D., Stark, H., and Courrèges-Lacoste, G. B.: Requirements for the GMES Atmosphere Service and ESA's implementation concept: Sentinels-4/-5 and -5p, Remote Sens. Environ., 120, 58–69, doi:10.1016/j.rse.2012.01.023, 2012.

IPCC Working Group 1, Stocker, T. F., Qin, D., Plattner, G.-K., Tignor, M., Allen, S. K., Boschung, J., Nauels, A., Xia, Y., Bex, V., and Midgley, P. M.: IPCC, 2013: Climate Change 2013: The Physical Science Basis. Contribution of Working Group I to the Fifth Assessment Report of the Intergovernmental Panel on Climate Change, IPCC, AR5, 1535, 2013.

Irie, H., Boersma, K. F., Kanaya, Y., Takashima, H., Pan, X., and Wang, Z. F.: Quantitative bias estimates for tropospheric NO_2 columns retrieved from SCIAMACHY, OMI, and GOME-2 using a common standard for East Asia, Atmos. Meas. Tech., 5, 2403–2411, doi:10.5194/amt-5-2403-2012, 2012.

Jia, B., Wang, Y., Yao, Y., and Xie, Y.: A new indictor on the impact of large-scale circulation on wintertime particulate matter pollution over China, Atmos. Chem. Phys. Discuss., 15, 19275–19304, doi:10.5194/acpd-15-19275-2015, 2015.

Khokhar, M. F., Frankenberg, C., Van Roozendael, M., Beirle, S., Kühl, S., Richter, A., Platt, U., and Wagner, T.: Satellite observations of atmospheric SO_2 from volcanic eruptions during the time-period of 1996–2002, Adv. Space Res., 36, 879–887, 2005.

Kim, S. W., Heckel, A., Frost, G. J., Richter, A., Gleason, J., Burrows, J. P., McKeen, S., Hsie, E. Y., Granier, C., and Trainer, M.: NO_2 columns in the western United States observed from space and simulated by a regional chemistry model and their implications for NO_x emissions, J. Geophys. Res.-Atmos., 114, D11301, doi:10.1029/2008JD011343, 2009.

Klimont, Z., Cofala, J., Xing, J., Wei, W., Zhang, C., Wang, S., Kejun, J., Bhandari, P., Mathur, R., Purohit, P., Rafaj, P., Chambers, A., Amann, M., and Hao, J.: Projections of SO_2, NO_x and carbonaceous aerosols emissions in Asia, Tellus B, 61, 602–617, doi:10.3402/tellusb.v61i4.16858, 2009.

Klimont, Z., Smith, S. J., and Cofala, J.: The last decade of global anthropogenic sulfur dioxide: 2000–2011 emissions, Environ. Res. Lett., 8, 014003, doi:10.1088/1748-9326/8/1/014003, 2013.

KNMI: Background information about the Row Anomaly in OMI, available at: http://www.knmi.nl/omi/research/product/rowanomaly-background.php (last access: 5 August 2015), 2012.

Konovalov, I. B., Beekmann, M., Richter, A., and Burrows, J. P.: Inverse modelling of the spatial distribution of NO_x emissions on a continental scale using satellite data, Atmos. Chem. Phys., 6, 1747–1770, doi:10.5194/acp-6-1747-2006, 2006.

Konovalov, I. B., Beekmann, M., Richter, A., Burrows, J. P., and Hilboll, A.: Multi-annual changes of NO_x emissions in megacity regions: nonlinear trend analysis of satellite measurement based estimates, Atmos. Chem. Phys., 10, 8481–8498, doi:10.5194/acp-10-8481-2010, 2010.

Krotkov, N. A., Cam, S. A., Krueger, A. J., Bhartia, P. K., and Yang, K.: Band residual difference algorithm for retrieval of SO_2 from the aura Ozone Monitoring Instrument (OMI), IEEE T. Geosci. Remote, 44, 1259–1266, doi:10.1109/TGRS.2005.861932, 2006.

Krotkov, N. A., McClure, B., Dickerson, R. R., Carn, S. A., Li, C., Bhartia, P. K., Yang, K., Krueger, A. J., Li, Z., Levelt, P. F., Chen, H., Wang, P., and Lu, D.: Validation of SO_2 retrievals from the Ozone Monitoring Instrument over NE China, J. Geophys. Res.-Atmos., 113, D16S40, doi:10.1029/2007JD008818, 2008.

Krueger, A. J.: Sighting of el chichon sulfur dioxide clouds with the Nimbus 7 Total Ozone Mapping Spectrometer, Science, 220, 1377–1379, doi:10.1126/science.220.4604.1377, 1983.

Lamsal, L. N., Martin, R. V., van Donkelaar, A., Steinbacher, M., Celarier, E. A., Bucsela, E., Dunlea, E. J., and Pinto, J. P.: Ground-level nitrogen dioxide concentrations inferred from the satellite-borne Ozone Monitoring Instrument, J. Geophys. Res.-Atmos., 113, D16308, doi:10.1029/2007JD009235, 2008.

Discussion Paper | Discussion Paper | Discussion Paper | Discussion Paper

Lamsal, L. N., Martin, R. V., Van Donkelaar, A., Celarier, E. A., Bucsela, E. J., Boersma, K. F., Dirksen, R., Luo, C., and Wang, Y.: Indirect validation of tropospheric nitrogen dioxide retrieved from the OMI satellite instrument: insight into the seasonal variation of nitrogen oxides at northern midlatitudes, J. Geophys. Res.-Atmos., 115, D05302, doi:10.1029/2009JD013351, 2010.

Lamsal, L. N., Martin, R. V., Padmanabhan, A., van Donkelaar, A., Zhang, Q., Sioris, C. E., Chance, K., Kurosu, T. P., and Newchurch, M. J.: Application of satellite observations for timely updates to global anthropogenic NO_x emission inventories, Geophys. Res. Lett., 38, L05810, doi:10.1029/2010GL046476, 2011.

Lamsal, L. N., Martin, R. V., Parrish, D. D., and Krotkov, N. A.: Scaling relationship for NO_2 pollution and urban population size: a satellite perspective, Environ. Sci. Technol., 47, 7855–7861, doi:10.1021/es400744g, 2013.

Lamsal, L. N., Duncan, B. N., Yoshida, Y., Krotkov, N. A., Pickering, K. E., Streets, D. G., and Lu, Z.: US NO_2 trends (2005–2013): EPA Air Quality System (AQS) data versus improved observations from the Ozone Monitoring Instrument (OMI), Atmos. Environ., 110, 130–143, doi:10.1016/j.atmosenv.2015.03.055, 2015.

Lee, C., Martin, R. V., Van Donkelaar, A., O'Byrne, G., Krotkov, N., Richter, A., Huey, L. G., and Holloway, J. S.: Retrieval of vertical columns of sulfur dioxide from SCIAMACHY and OMI: Air mass factor algorithm development, validation, and error analysis, J. Geophys. Res.-Atmos., 114, D22303, doi:10.1029/2009JD012123, 2009.

Lee, C., Martin, R. V., Van Donkelaar, A., Lee, H., Dickerson, R. R., Hains, J. C., Krotkov, N., Richter, A., Vinnikov, K., and Schwab, J. J.: SO_2 emissions and lifetimes: estimates from inverse modeling using in situ and global, space-based (SCIAMACHY and OMI) observations, J. Geophys. Res.-Atmos., 116, D06304, doi:10.1029/2010JD014758, 2011.

Lee, C. J., Martin, R. V., Henze, D. K., Brauer, M., Cohen, A., and Van Donkelaar, A.: Response of global particulate-matter-related mortality to changes in local precursor emissions, Environ. Sci. Technol., 49, 4335–4344, doi:10.1021/acs.est.5b00873, 2015.

Lelieveld, J., Beirle, S., Hörmann, C., Stenchikov, G., and Wagner, T.: Abrupt recent trend changes in atmospheric nitrogen dioxide over the Middle East, Sci. Adv., 1, 2–6, doi:10.1126/sciadv.1500498, 2015.

Leue, C., Wenig, M., Wagner, T., Klimm, O., Platt, U., and Jähne, B.: Quantitative analysis of NO_x emissions from Global Ozone Monitoring Experiment satellite image sequences, J. Geophys. Res., 106, 5493, doi:10.1029/2000JD900572, 2001.

Levelt, P. F., Hilsenrath, E., Leppelmeier, G. W., Van Den Oord, G. H. J., Bhartia, P. K., Tamminen, J., De Haan, J. F., and Veefkind, J. P.: Science objectives of the Ozone Monitoring Instrument, IEEE T. Geosci. Remote, 44, 1199–1208, 2006a.

Levelt, P. F., Van Den Oord, G. H. J., Dobber, M. R., Mälkki, A., Visser, H., De Vries, J., Stammes, P., Lundell, J. O. V., and Saari, H.: The Ozone Monitoring Instrument, IEEE T. Geosci. Remote, 44, 1093–1101, 2006b.

Li, C., Marufu, L. T., Dickerson, R. R., Li, Z., Wen, T., Wang, Y., Wang, P., Chen, H., and Stehr, J. W.: In situ measurements of trace gases and aerosol optical properties at a rural site in northern China during East Asian Study of Tropospheric Aerosols: an International Regional Experiment 2005, J. Geophys. Res., 112, D22S04, doi:10.1029/2006JD007592, 2007.

Li, C., Zhang, Q., Krotkov, N. A., Streets, D. G., He, K., Tsay, S.-C., and Gleason, J. F.: Recent large reduction in sulfur dioxide emissions from Chinese power plants observed by the Ozone Monitoring Instrument, Geophys. Res. Lett., 37, 1–6, doi:10.1029/2010GL042594, 2010.

Li, C., Joiner, J., Krotkov, N. A., and Bhartia, P. K.: A fast and sensitive new satellite SO_2 retrieval algorithm based on principal component analysis: application to the ozone monitoring instrument, Geophys. Res. Lett., 40, 6314–6318, doi:10.1002/2013GL058134, 2013.

Liu, Y., Chen, X., Huang, S., Tian, L., Lu, Y., Mei, Y., Ren, M., Li, N., Liu, L., and Xiang, H.: Association between air pollutants and cardiovascular disease mortality in Wuhan, China, Int. J. Environ. Res. Public Health, 12, 3506–3516, doi:10.3390/ijerph120403506, 2015.

Lookman, A. A. and Rubin, E. S.: Barriers to adopting least-cost particulate control strategies for Indian power plants, Energy Policy, 26, 1053–1063, doi:10.1016/S0301-4215(98)00049-4, 1998.

Lu, Z. and Streets, D. G.: Increase in NO_x emissions from Indian thermal power plants during 1996–2010: unit-based inventories and multisatellite observations, Environ. Sci. Technol., 46, 7463–7470, doi:10.1021/es300831w, 2012.

Lu, Z., Streets, D. G., Zhang, Q., Wang, S., Carmichael, G. R., Cheng, Y. F., Wei, C., Chin, M., Diehl, T., and Tan, Q.: Sulfur dioxide emissions in China and sulfur trends in East Asia since 2000, Atmos. Chem. Phys., 10, 6311–6331, doi:10.5194/acp-10-6311-2010, 2010.

Lu, Z., Zhang, Q., and Streets, D. G.: Sulfur dioxide and primary carbonaceous aerosol emissions in China and India, 1996–2010, Atmos. Chem. Phys., 11, 9839–9864, doi:10.5194/acp-11-9839-2011, 2011.

Title Page

Abstract | Introduction

Conclusions | References

Tables | Figures

|◄ | ►|

◄ | ►

Back | Close

Full Screen / Esc

Printer-friendly Version

Interactive Discussion

Lu, Z., Streets, D. G., De Foy, B., and Krotkov, N. A.: Ozone monitoring instrument observations of interannual increases in SO_2 emissions from Indian coal-fired power plants during 2005–2012, Environ. Sci. Technol., 47, 13993–14000, doi:10.1021/es4039648, 2013.

Lu, Z., Streets, D. G., de Foy, B., Lamsal, L. N., Duncan, B. N., and Xing, J.: Emissions of nitrogen oxides from US urban areas: estimation from Ozone Monitoring Instrument retrievals for 2005–2014, Atmos. Chem. Phys. Discuss., 15, 14961–15003, doi:10.5194/acpd-15-14961-2015, 2015.

Martin, R. V.: Satellite remote sensing of surface air quality, Atmos. Environ., 42, 7823–7843, doi:10.1016/j.atmosenv.2008.07.018, 2008a.

Martin, R. V.: Satellite remote sensing of surface air quality, Atmos. Environ., 42, 7823–7843, doi:10.1016/j.atmosenv.2008.07.018, 2008b.

Martin, R. V., Chance, K., Jacob, D. J., Kurosu, T. P., Spurr, R. J. D., Bucsela, E., Gleason, J. F., Palmer, P. I., Bey, I., Fiore, A. M., Li, Q., Yantosca, R. M., and Koelemeijer, R. B. A.: An improved retrieval of tropospheric nitrogen dioxide from GOME, J. Geophys. Res.-Atmos., 107, 4437, doi:10.1029/2001JD001027, 2002.

McLinden, C. A., Fioletov, V., Boersma, K. F., Krotkov, N., Sioris, C. E., Veefkind, J. P., and Yang, K.: Air quality over the Canadian oil sands: a first assessment using satellite observations, Geophys. Res. Lett., 39, L04804, doi:10.1029/2011GL050273, 2012.

McLinden, C. A., Fioletov, V., Boersma, K. F., Kharol, S. K., Krotkov, N., Lamsal, L., Makar, P. A., Martin, R. V., Veefkind, J. P., and Yang, K.: Improved satellite retrievals of NO_2 and SO_2 over the Canadian oil sands and comparisons with surface measurements, Atmos. Chem. Phys., 14, 3637–3656, doi:10.5194/acp-14-3637-2014, 2014.

Mebust, A. K. and Cohen, R. C.: Space-based observations of fire NO_x emission coefficients: a global biome-scale comparison, Atmos. Chem. Phys., 14, 2509–2524, doi:10.5194/acp-14-2509-2014, 2014.

MEP: The airborne pollution prevention and control action plan, available at: http://english.mep.gov.cn/News_service/infocus/201309/t20130924_260707.htm (last access: 26 August 2015), 2013.

Mijling, B. and Van Der A, R. J.: Using daily satellite observations to estimate emissions of short-lived air pollutants on a mesoscopic scale, J. Geophys. Res.-Atmos., 117, 1–20, doi:10.1029/2012JD017817, 2012.

Mijling, B., van der A, R. J., Boersma, K. F., Van Roozendael, M., De Smedt, I., and Kelder, H. M.: Reductions of NO_2 detected from space during the 2008 Beijing Olympic Games, Geophys. Res. Lett., 36, L13801, doi:10.1029/2009GL038943, 2009.

Miyazaki, K., Eskes, H. J., and Sudo, K.: Global NO_x emission estimates derived from an assimilation of OMI tropospheric NO_2 columns, Atmos. Chem. Phys., 12, 2263–2288, doi:10.5194/acp-12-2263-2012, 2012.

Napelenok, S. L., Pinder, R. W., Gilliland, A. B., and Martin, R. V.: A method for evaluating spatially-resolved NO_x emissions using Kalman filter inversion, direct sensitivities, and space-based NO_2 observations, Atmos. Chem. Phys., 8, 5603–5614, doi:10.5194/acp-8-5603-2008, 2008.

Nowlan, C. R., Martin, R. V., Philip, S., Lamsal, L. N., Krotkov, N. A., Marais, E. A., Wang, S., and Zhang, Q.: Global dry deposition of nitrogen dioxide and sulfur dioxide inferred from space-based measurements, Global Biogeochem. Cy., 28, 1025–1043, doi:10.1002/2014GB004805, 2014.

Oetjen, H., Baidar, S., Krotkov, N. A., Lamsal, L. N., Lechner, M., and Volkamer, R.: Airborne MAX-DOAS measurements over California: testing the NASA OMI tropospheric NO_2 product, J. Geophys. Res.-Atmos., 118, 7400–7413, doi:10.1002/jgrd.50550, 2013.

Pourzamani, H., Aliyan, T., and Daryalal, M.: Evaluation of SO_2 level in the ambient air of Khark Island, Int. J. Environ. Health Eng. , 1, 39, doi:10.4103/2277-9183.102368, 2012.

Reuter, M., Buchwitz, M., Hilboll, A., Richter, A., Schneising, O., Hilker, M., Heymann, J., Bovensmann, H., and Burrows, J. P.: Decreasing emissions of NO_x relative to CO_2 in East Asia inferred from satellite observations, Nat. Geosci., 7, 792–795, doi:10.1038/ngeo2257, 2014.

Richter, A. and Burrows, J. P.: Tropospheric NO_2 from GOME measurements, Adv. Space Res., 2, 1–11, 2002.

Richter, A., Burrows, J. P., Nüss, H., Granier, C., and Niemeier, U.: Increase in tropospheric nitrogen dioxide over China observed from space, Nature, 437, 129–132, doi:10.1038/nature04092, 2005.

Richter, A., Begoin, M., Hilboll, A., and Burrows, J. P.: An improved NO_2 retrieval for the GOME-2 satellite instrument, Atmos. Meas. Tech., 4, 1147–1159, doi:10.5194/amt-4-1147-2011, 2011.

Richter, A., Hillbol, A., and Burrows, J. P.: Improving S5P NO_2 retrievals, available at: http://seom.esa.int/atmos2015/page_presentations.php (last access: 27 September 2015), 2015.

Title Page

Abstract | Introduction

Conclusions | References

Tables | Figures

◄ | ►

◄ | ►

Back | Close

Full Screen / Esc

Printer-friendly Version

Interactive Discussion

Rix, M., Valks, P., Hao, N., Loyola, D., Schlager, H., Huntrieser, H., Flemming, J., Koehler, U., Schumann, U., and Inness, A.: Volcanic SO_2, BrO and plume height estimations using GOME-2 satellite measurements during the eruption of Eyjafjallajökull in May 2010, J. Geophys. Res.-Atmos., 117, D00U19, doi:10.1029/2011JD016718, 2012.

Russell, A. R., Valin, L. C., and Cohen, R. C.: Trends in OMI NO_2 observations over the United States: effects of emission control technology and the economic recession, Atmos. Chem. Phys., 12, 12197–12209, doi:10.5194/acp-12-12197-2012, 2012.

Schneider, P. and Van Der A, R. J.: A global single-sensor analysis of 2002–2011 tropospheric nitrogen dioxide trends observed from space, J. Geophys. Res.-Atmos., 117, D16309, doi:10.1029/2012JD017571, 2012.

Schneider, P., Lahoz, W. A., and van der A, R.: Recent satellite-based trends of tropospheric nitrogen dioxide over large urban agglomerations worldwide, Atmos. Chem. Phys., 15, 1205–1220, doi:10.5194/acp-15-1205-2015, 2015.

Schoeberl, M. R., Douglass, A. R., Hilsenrath, E., Bhartia, P. K., Beer, R., Waters, J. W., Gunson, M. R., Froidevaux, L., Gille, J. C., Barnett, J. J., Levelt, P. F., and DeCola, P.: Overview of the EOS aura mission, IEEE T. Geosci. Remote, 44, 1066–1072, doi:10.1109/TGRS.2005.861950, 2006.

Schumann, U. and Huntrieser, H.: The global lightning-induced nitrogen oxides source, Atmos. Chem. Phys., 7, 3823–3907, doi:10.5194/acp-7-3823-2007, 2007.

Seinfeld, J. H. and Pandis, S. N.: Atmospheric Chemistry and Physics: From Air Pollution to Climate Change, 2nd Edn. 2006, John Wiley & Sons, Hoboken, New Jersey, 2006.

Simon, H., Reff, A., Wells, B., Xing, J., and Frank, N.: Ozone trends across the United States over a period of decreasing NO_x and VOC emissions, Environ. Sci. Technol., 49, 186–195, doi:10.1021/es504514z, 2015.

Smith, S. J., van Aardenne, J., Klimont, Z., Andres, R. J., Volke, A., and Delgado Arias, S.: Anthropogenic sulfur dioxide emissions: 1850–2005, Atmos. Chem. Phys., 11, 1101–1116, doi:10.5194/acp-11-1101-2011, 2011a.

Smith, S. J., van Aardenne, J., Klimont, Z., Andres, R. J., Volke, A., and Delgado Arias, S.: Anthropogenic sulfur dioxide emissions: 1850–2005, Atmos. Chem. Phys., 11, 1101–1116, doi:10.5194/acp-11-1101-2011, 2011b.

Solomon, P. A., Crumpler, D., Flanagan, J. B., Jayanty, R. K. M., Rickman, E. E., and McDade, C. E.: US national $PM_{2.5}$ Chemical Speciation Monitoring Networks-CSN and IM-

Title Page

Abstract | Introduction

Conclusions | References

Tables | Figures

◀ | ▶

◀ | ▶

Back | Close

Full Screen / Esc

Printer-friendly Version

Interactive Discussion

PROVE: description of networks, J. Air Waste Manage., 64, 1410–1438, available at: http://www.ncbi.nlm.nih.gov/pubmed/25562937 (last access: 7 August 2015), 2014.

Stavrakou, T., Müller, J.-F., Boersma, K. F., De Smedt, I., and van der A, R. J.: Assessing the distribution and growth rates of NO_x emission sources by inverting a 10-year record of NO_2 satellite columns, Geophys. Res. Lett., 35, L10801, doi:10.1029/2008GL033521, 2008.

Streets, D. G., Canty, T., Carmichael, G. R., de Foy, B., Dickerson, R. R., Duncan, B. N., Edwards, D. P., Haynes, J. A., Henze, D. K., Houyoux, M. R., Jacob, D. J., Krotkov, N. A., Lamsal, L. N., Liu, Y., Lu, Z., Martin, R. V., Pfister, G. G., Pinder, R. W., Salawitch, R. J., and Wecht, K. J.: Emissions estimation from satellite retrievals: a review of current capability, Atmos. Environ., 77, 1011–1042, doi:10.1016/j.atmosenv.2013.05.051, 2013.

Theys, N., De Smedt, I., van Gent, J., Danckaert, T., Wang, T., Hendrick, F., Stavrakou, T., Bauduin, S., Clarisse, L., Li, C., Krotkov, N., Yu, H., Brenot, H., and Van Roozendael, M.: Sulfur dioxide vertical column DOAS retrievals from the Ozone Monitoring Instrument: global observations and comparison to ground-based and satellite data, J. Geophys. Res.-Atmos., 120, 2470–2491, doi:10.1002/2014JD022657, 2015.

Tian, H., Qiu, P., Cheng, K., Gao, J., Lu, L., Liu, K., and Liu, X.: Current status and future trends of SO_2 and NO_x pollution during the 12th FYP period in Guiyang city of China, Atmos. Environ., 69, 273–280, doi:10.1016/j.atmosenv.2012.12.033, 2013.

Tong, D. Q., Lamsal, L., Pan, L., Ding, C., Kim, H., Lee, P., Chai, T., Pickering, K. E., and Stajner, I.: Long-term NO_x trends over large cities in the United States during the great recession: comparison of satellite retrievals, ground observations, and emission inventories, Atmos. Environ., 107, 70–84, doi:10.1016/j.atmosenv.2015.01.035, 2015.

Twohy, C. H.: Nitrogenated organic aerosols as cloud condensation nuclei, Geophys. Res. Lett., 32, L19805, doi:10.1029/2005GL023605, 2005.

US Department of Veterans Affairs: Sulfur Fire at Mishraq State Sulfur Mine – Public Health, available at: http://www.publichealth.va.gov/exposures/mishraq-sulfur-fire/index.asp (last access: 25 August 2015), 2015.

US EIA: Coal plants without scrubbers account for a majority of US SO_2 emissions – today in energy, U.S. Energy Information Administration (EIA), available at: http://www.eia.gov/todayinenergy/detail.cfm?id=4410 (last access: 9 August 2015), 2010.

US EPA: National Emissions Inventory (NEI) Air Pollutant Emissions Trends Data, available at: http://www.epa.gov/ttnchie1/trends/ (last access: 7 August 2015), 2014.

Title Page

Abstract | Introduction

Conclusions | References

Tables | Figures

|◀ | ▶|

◀ | ▶

Back | Close

Full Screen / Esc

Printer-friendly Version

Interactive Discussion

US EPA: Six Common Air Pollutants, Air and Radiation, US EPA, available at: http://www3.epa.gov/ttn/chief/trends/ (last access: 27 September 2015), 2015.

Valin, L. C., Russell, A. R., and Cohen, R. C.: Variations of OH radical in an urban plume inferred from NO_2 column measurements, Geophys. Res. Lett., 40, 1856–1860, doi:10.1002/grl.50267, 2013.

Valks, P., Pinardi, G., Richter, A., Lambert, J.-C., Hao, N., Loyola, D., Van Roozendael, M., and Emmadi, S.: Operational total and tropospheric NO_2 column retrieval for GOME-2, Atmos. Meas. Tech., 4, 1491–1514, doi:10.5194/amt-4-1491-2011, 2011.

Van der A, R. J., Peters, D. H. M. U., Eskes, H., Boersma, K. F., Van Roozendael, M., De Smedt, I., and Kelder, H. M.: Detection of the trend and seasonal variation in tropospheric NO_2 over China, J. Geophys. Res.-Atmos., 111, 1–10, doi:10.1029/2005JD006594, 2006.

Van der A, R. J., Eskes, H. J., Boersma, K. F., van Noije, T. P. C., Van Roozendael, M., De Smedt, I., Peters, D. H. M. U., and Meijer, E. W.: Trends, seasonal variability and dominant NO_x source derived from a ten year record of NO_2 measured from space, J. Geophys. Res., 113, D04302, doi:10.1029/2007JD009021, 2008.

Vautard, R., Cattiaux, J., Yiou, P., Thépaut, J.-N., and Ciais, P.: Northern Hemisphere atmospheric stilling partly attributed to an increase in surface roughness, Nat. Geosci., 3, 756–761, doi:10.1038/ngeo979, 2010.

Veefkind, J. P., Aben, I., McMullan, K., Förster, H., de Vries, J., Otter, G., Claas, J., Eskes, H. J., de Haan, J. F., Kleipool, Q., van Weele, M., Hasekamp, O., Hoogeveen, R., Landgraf, J., Snel, R., Tol, P., Ingmann, P., Voors, R., Kruizinga, B., Vink, R., Visser, H., and Levelt, P. F.: TROPOMI on the ESA Sentinel-5 Precursor: a GMES mission for global observations of the atmospheric composition for climate, air quality and ozone layer applications, Remote Sens. Environ., 120, 70–83, doi:10.1016/j.rse.2011.09.027, 2012.

Vestreng, V., Ntziachristos, L., Semb, A., Reis, S., Isaksen, I. S. A., and Tarrasón, L.: Evolution of NO_x emissions in Europe with focus on road transport control measures, Atmos. Chem. Phys., 9, 1503–1520, doi:10.5194/acp-9-1503-2009, 2009.

Vinken, G. C. M., Boersma, K. F., van Donkelaar, A., and Zhang, L.: Constraints on ship NO_x emissions in Europe using GEOS-Chem and OMI satellite NO_2 observations, Atmos. Chem. Phys., 14, 1353–1369, doi:10.5194/acp-14-1353-2014, 2014a.

Vinken, G. C. M., Boersma, K. F., Maasakkers, J. D., Adon, M., and Martin, R. V.: Worldwide biogenic soil NO_x emissions inferred from OMI NO_2 observations, Atmos. Chem. Phys., 14, 10363–10381, doi:10.5194/acp-14-10363-2014, 2014b.

Title Page

Abstract | Introduction

Conclusions | References

Tables | Figures

|◄ | ►|

◄ | ►

Back | Close

Full Screen / Esc

Printer-friendly Version

Interactive Discussion

Witte, J. C., Schoeberl, M. R., Douglass, A. R., Gleason, J. F., Krotkov, N. A., Gille, J. C., Pickering, K. E., and Livesey, N.: Satellite observations of changes in air quality during the 2008 Beijing Olympics and Paralympics, Geophys. Res. Lett., 36, L17803, doi:10.1029/2009GL039236, 2009.

Zhang, Q., Streets, D. G., He, K., Wang, Y., Richter, A., Burrows, J. P., Uno, I., Jang, C. J., Chen, D., Yao, Z., and Lei, Y.: NO_x emission trends for China, 1995–2004: the view from the ground and the view from space, J. Geophys. Res.-Atmos., 112, D22306, doi:10.1029/2007JD008684, 2007.

Zhang, Q., Streets, D. G., and He, K.: Satellite observations of recent power plant construction in Inner Mongolia, China, Geophys. Res. Lett., 36, L15809, doi:10.1029/2009GL038984, 2009.

Zhang, X.-P. and Cheng, X.-M.: Energy consumption, carbon emissions, and economic growth in China, Ecol. Econ., 68, 2706–2712, doi:10.1016/j.ecolecon.2009.05.011, 2009.

Zhao, B., Wang, S., Wang, J., Fu, J. S., Liu, T., Xu, J., Fu, X., and Hao, J.: Impact of national NO_x and SO_2 control policies on particulate matter pollution in China, Atmos. Environ., 77, 453–463, doi:10.1016/j.atmosenv.2013.05.012, 2013.

Zhou, Y., Brunner, D., Boersma, K. F., Dirksen, R., and Wang, P.: An improved tropospheric NO_2 retrieval for OMI observations in the vicinity of mountainous terrain, Atmos. Meas. Tech., 2, 401–416, doi:10.5194/amt-2-401-2009, 2009.

Zhou, Y., Brunner, D., Hueglin, C., Henne, S., and Staehelin, J.: Changes in OMI tropospheric NO_2 columns over Europe from 2004 to 2009 and the influence of meteorological variability, Atmos. Environ., 46, 482–495, doi:10.1016/j.atmosenv.2011.09.024, 2012.

Zyrichidou, I., Koukouli, M. E., Balis, D. S., Katragkou, E., Poupkou, A., Kioutsioukis, I., Markakis, K., Melas, D., Van Der A, R., Boersma, F. K., and Van Roozendael, M.: Comparison of satellite NO_2 observations with high resolution model simulations over the Balkan Peninsula, in: AIP Conference Proceedings, Vol. 1203, 632–637, 2010.

Zyrichidou, I., Koukouli, M. E., Balis, D. S., Kioutsioukis, I., Poupkou, A., Katragkou, E., Melas, D., Boersma, K. F., and van Roozendael, M.: Evaluation of high resolution simulated and OMI retrieved tropospheric NO_2 column densities over southeastern Europe, Atmos. Res., 122, 55–66, doi:10.1016/j.atmosres.2012.10.028, 2013.

Title Page

Abstract | Introduction

Conclusions | References

Tables | Figures

|◄ | ►|

◄ | ►

Back | Close

Full Screen / Esc

Printer-friendly Version

Interactive Discussion

Table A1. Filtering transient volcanic clouds.

Region	Threshold (DU)	Days excluded (2005–2014)
Eastern US	5	97
Eastern Europe	8	72
Eastern China	10	71
India	8	58
Middle East	8	10
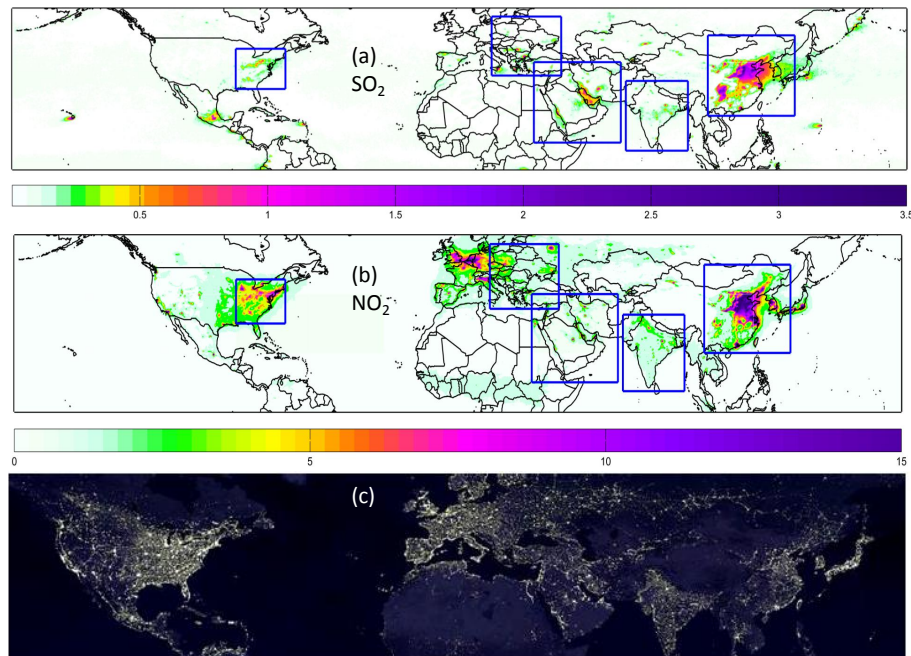
Figure 1. OMI-derived maps of PBL SO$_2$ in Dobson Units [DU] **(a)** and tropospheric NO$_2$ columns in [10^{15} molecules cm^{-2}] **(b)** for 2005–2007 show enhanced pollution levels around major cities and industrial centers, seen also in the "Earth at Night" (city lights) map **(c)**, courtesy of Aura EPO team.

Title Page

Abstract | Introduction

Conclusions | References

Tables | Figures

|◄ | ►|

◄ | ►

Back | Close

Full Screen / Esc

Printer-friendly Version

Interactive Discussion
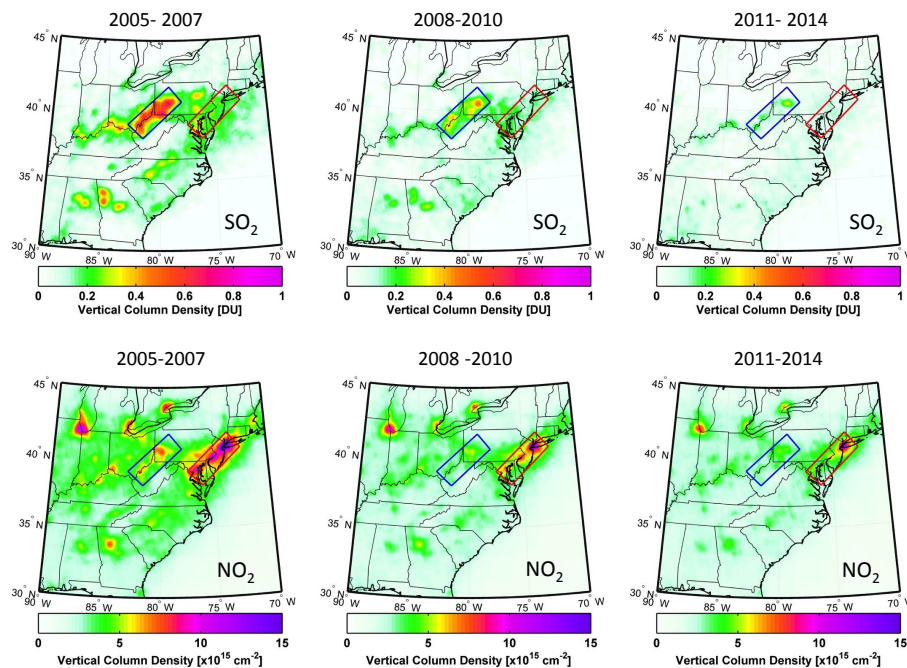
Figure 2. Multiyear average OMI SO$_2$ (top) and tropospheric NO$_2$ (bottom) regional maps over eastern US for 3 periods: 2005–2007, 2008–2010 and 2011–2014. Blue box outlines Ohio River Valley and SW Pennsylvania (ORV) region with largest SO$_2$ emissions from coal-fired power plants. Red box outlines megalopolis from Washington, DC to New York along the I-95 interstate highway (I-95 corridor) with largest NO$_2$ from mobile sources.

Title Page

Abstract   Introduction

Conclusions   References

Tables   Figures

◄   ►

Back   Close

Full Screen / Esc

Printer-friendly Version

Interactive Discussion
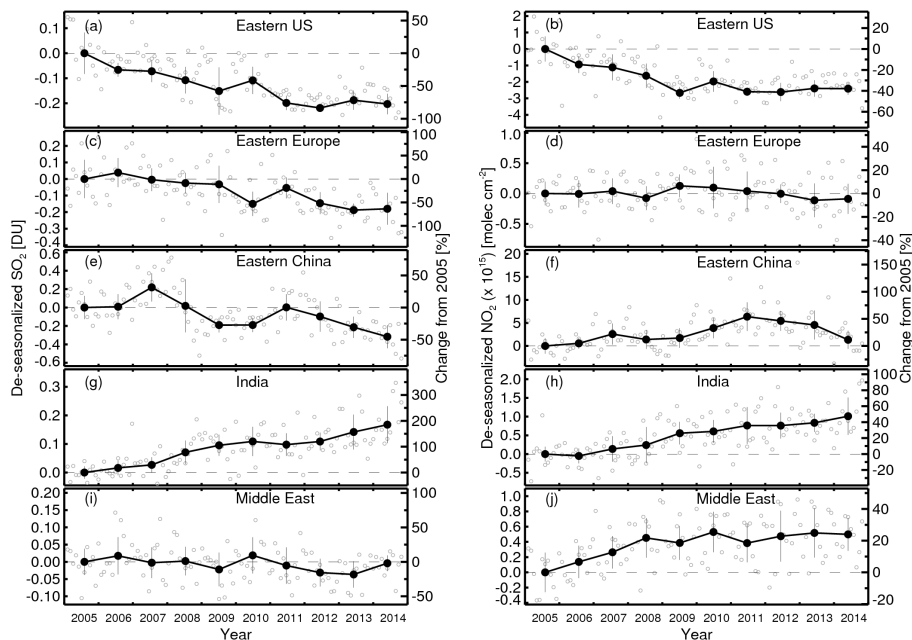
Figure 3. Relative changes (compared to 2005) in OMI PBL SO_2 columns (left) and tropospheric NO_2 columns (right) over 5 world's most polluted regions: **(a and b)**: Ohio River Valley and western Pennsylvania (ORV) in eastern US (ORV – blue box in Fig. 2); **(c and d)**: Maritsa Iztok Power Plants in Bulgaria (blue box in Fig. 4); **(e and f)**: North China Plane (NCP – blue box in Fig. 5); **(g and h)**: NE India (blue box in Fig. 6); **(i and j)**: Persian Gulf (blue box in Fig. 7). Gray circles show de-seasonalized monthly columns (see details in Supplement). Black filled circles show annual means. Vertical bars show standard deviations.

Title Page

Abstract | Introduction

Conclusions | References

Tables | Figures

|◄ | ►|

◄ | ►

Back | Close

Full Screen / Esc

Printer-friendly Version

Interactive Discussion

Full Screen / Esc

Printer-friendly Version

Interactive Discussion
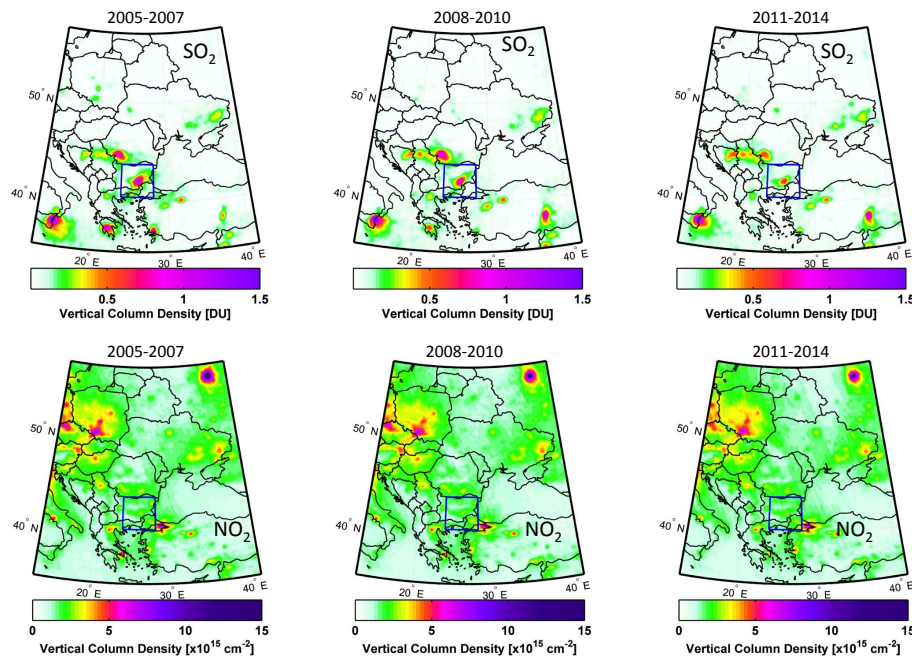
Figure 4. Same as Fig. 2, but for Eastern Europe. The largest SO$_2$ source in the domain is the Etna volcano in Sicily, Italy. The blue box is centered on SO$_2$ polluted area around Maritsa Iztok coal mining region and the largest coal-fired power plant in southeastern Bulgaria.
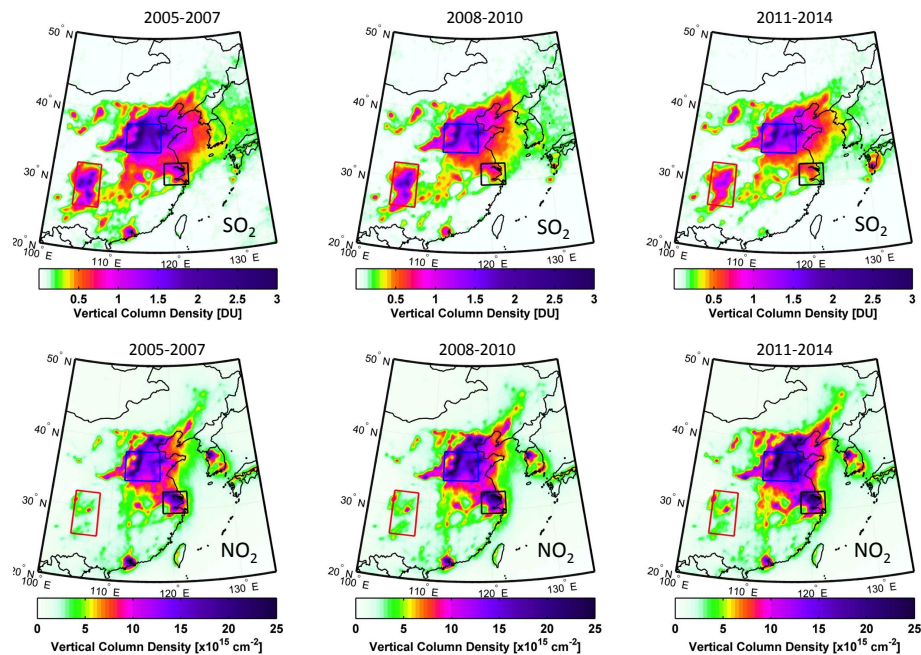
Figure 5. Similar to Fig. 2 but for eastern China. Blue box outlines North China Plane (NCP) also represented in Fig. 3, red box – Sichuan Basin (SB) and black box represent Yangtze River Delta (YRD). The boxes are also shown in Figs. S1, S3 and S4.
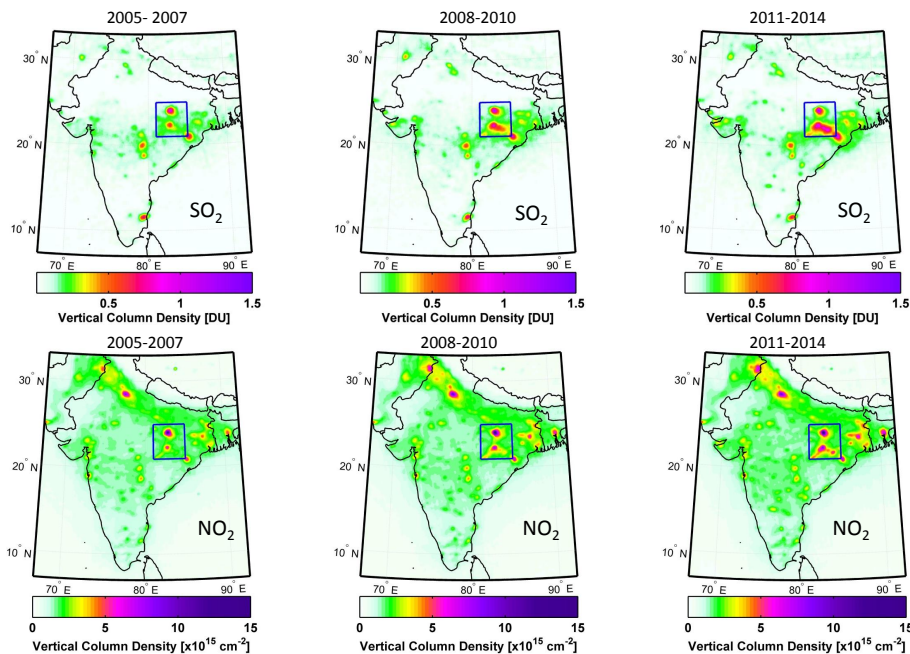
Figure 6. Similar to Fig. 2 but for India. Blue box outlines industrial regions in Chhattisgarh and Odisha, one of India's most active areas in terms of building new coal-fired power plants. The region is shown in Fig. 3.
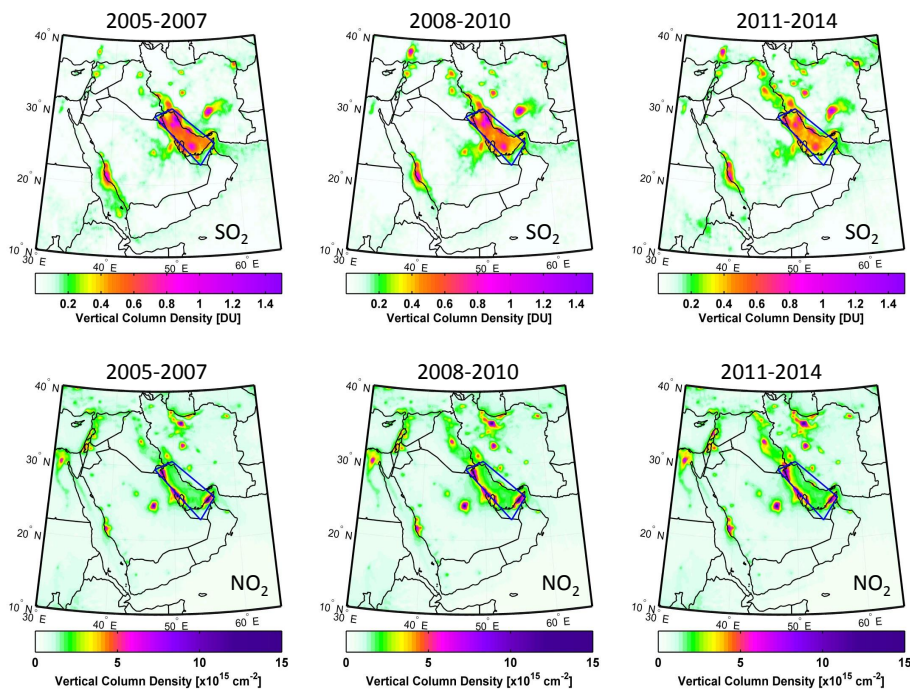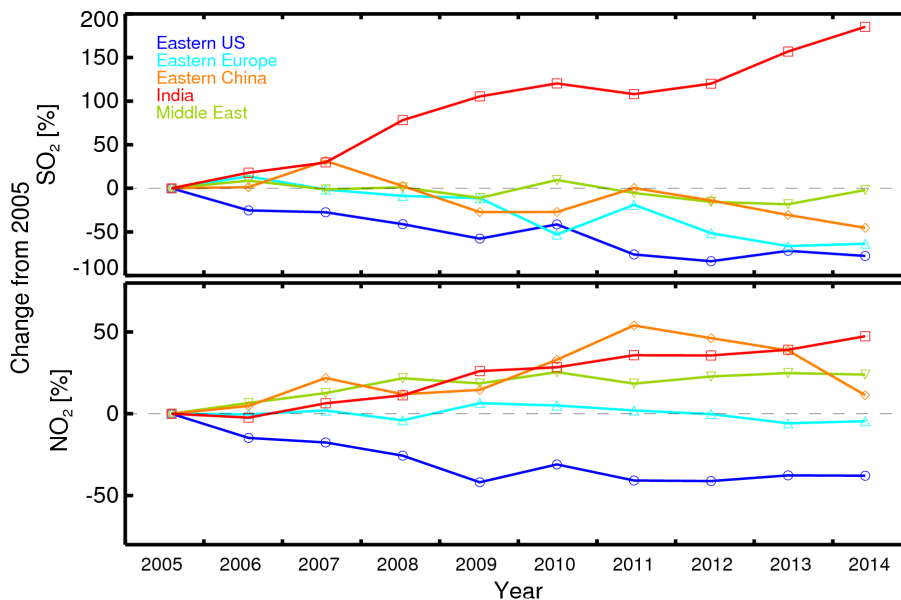
Figure 7. Similar to Fig. 2 but for the Middle East. Blue box outlines Persian Gulf region with high SO$_2$ and NO$_2$ levels due to oil and gas operations.

Figure 8. Percent change in OMI annual average columns: SO$_2$ (top) and NO$_2$ (bottom) over the world's most polluted regions.